Biogeosciences Discuss., 10, 16491–16549, 2013
www.biogeosciences-discuss.net/10/16491/2013/
doi:10.5194/bgd-10-16491-2013

Biogeosciences
Discussions
Open Access

A satellite data driven biophysical modeling approach for estimating northern peatland and tundra CO_2 and CH_4 fluxes

J. D. Watts[1,2], J. S. Kimball[1,2], F.-J. W. Parmentier[3], T. Sachs[4], J. Rinne[5], D. Zona[6,7], W. Oechel[7], T. Tagesson[8], M. Jackowicz-Korczyński[3], and M. Aurela[9]

[1]Flathead Lake Biological Station, The University of Montana, 32125 Bio Station Lane, Polson, MT, USA
[2]Numerical Terradynamic Simulation Group, CHCB 428, 32 Campus Drive, The University of Montana, Missoula, MT, USA
[3]Department of Physical Geography and Ecosystem Science, Lund University, Sölvegatan 12, 223 62, Lund, Sweden
[4]Helmholtz Centre Potsdam – GFZ German Research Centre for Geosciences, Telegrafenberg, 14473 Potsdam, Germany
[5]Department of Physics, P.O. Box 48, 00014 University of Helsinki, Finland
[6]Department of Animal and Plant Science, University of Sheffield, Sheffield, UK
[7]Department of Biology, San Diego State University, San Diego, CA, USA

[8]Department of Geography and Geology, University of Copenhagen, Øster Voldgade 10, 1350 København, Denmark
[9]Finnish Meteorological Institute, Climate Change Research, P.O. Box 503, 00101, Helsinki, Finland

Received: 5 September 2013 – Accepted: 11 October 2013 – Published: 25 October 2013

Correspondence to: J. D. Watts (jennifer.watts@ntsg.umt.edu)

Published by Copernicus Publications on behalf of the European Geosciences Union.

Abstract

The northern terrestrial net ecosystem carbon balance (NECB) is contingent on inputs from vegetation gross primary productivity (GPP) to offset ecosystem respiration (R_{eco}) of carbon dioxide (CO_2) and methane (CH_4) emissions, but an effective framework to monitor the regional Arctic NECB is lacking. We modified a terrestrial carbon flux (TCF) model developed for satellite remote sensing applications to estimate peatland and tundra CO_2 and CH_4 fluxes over a pan-Arctic network of eddy covariance (EC) flux tower sites. The TCF model estimates GPP, CO_2 and CH_4 emissions using either in-situ or remote sensing based climate data as input. TCF simulations driven using in-situ data explained > 70 % of the r^2 variability in 8 day cumulative EC measured fluxes. Model simulations using coarser satellite (MODIS) and reanalysis (MERRA) data as inputs also reproduced the variability in the EC measured fluxes relatively well for GPP ($r^2 = 0.75$), R_{eco} ($r^2 = 0.71$), net ecosystem CO_2 exchange (NEE, $r^2 = 0.62$) and CH_4 emissions ($r^2 = 0.75$). Although the estimated annual CH_4 emissions were small (< 18 g C m^{-2} yr^{-1}) relative to R_{eco} (> 180 g C m^{-2} yr^{-1}), they reduced the across-site NECB by 23 % and contributed to a global warming potential of approximately 165 ± 128 g CO_2eq m^{-2} yr^{-1} when considered over a 100 yr time span. This model evaluation indicates a strong potential for using the TCF model approach to document landscape scale variability in CO_2 and CH_4 fluxes, and to estimate the NECB for northern peatland and tundra ecosystems.

1 Introduction

Northern peatland and tundra ecosystems are important components of the terrestrial carbon cycle and store over half of the global soil organic carbon reservoir in seasonally frozen and permafrost soils (Hugelius et al., 2013). However, these systems are becoming increasingly vulnerable to carbon losses as carbon dioxide (CO_2) and methane (CH_4) emissions, resulting from climate warming and changes in the terrestrial water

BGD
10, 16491–16549, 2013

Title Page
Abstract | Introduction
Conclusions | References
Tables | Figures
◀| |▶
◀ ▶
Back | Close
Full Screen / Esc
Printer-friendly Version
Interactive Discussion

balance (Kane et al., 2012; Kim et al., 2012) that can increase soil carbon decomposition. Recent net CO_2 exchange in northern tundra and peatland ecosystems varies from a sink of 291 $Tg\,C\,yr^{-1}$ to a source of 80 $Tg\,C\,yr^{-1}$, when considering the substantial uncertainty in regional estimates using scaled flux observations, atmospheric inversions, and ecosystem process models (McGuire et al., 2012). The magnitude of carbon sink largely depends on the balance between carbon uptake by vegetation productivity and losses from soil mineralization and respiration processes. High latitude warming can increase ecosystem carbon uptake by reducing cold-temperature constraints on plant carbon assimilation and growth (Hudson et al., 2011; Elmendorf et al., 2012). Soil warming also accelerates carbon losses due to the exponential effects of temperature on soil respiration, whereas wet and inundated conditions shift microbial activity towards anaerobic consumption pathways that are relatively slow but can result in substantial CH_4 production (Moosavi and Crill, 1997; Merbold et al., 2009). Regional wetting across the Arctic (Watts et al., 2012; Zhang et al., 2012a) may increase CH_4 emissions, which have a radiative warming potential at least 25 times more potent than CO_2 per unit mass over a 100 yr time horizon (Boucher et al., 2009). The northern latitudes already contain over 50 % of global wetlands and recent increases in atmospheric CH_4 concentrations have been attributed to heightened gas emissions in these areas during periods of warming (Dlugokencky et al., 2009; Dolman et al., 2010). Northern peatland and tundra ($\geq 50^\circ$ N) reportedly contribute between 8–79 Tg C in CH_4 emissions each year, but these fluxes have been difficult to constrain due to uncertainty in the parameterization of biogeochemical models, the regional characterization of wetland extent and water table depth, and a scarcity of ecosystem scale CH_4 emission observations (Petrescu et al., 2010; Riley et al., 2011; Spahni et al., 2011; McGuire et al., 2012; Meng et al., 2012).

Ecosystem studies using chamber and eddy covariance (EC) methods continue to provide direct measurements of CO_2 and CH_4 fluxes and add valuable insight into the environmental constraints on these processes. However, extrapolating localized carbon fluxes to regional scales has proven difficult and is severely constrained by the extremely sparse in-situ monitoring network and the large spatial extent and heterogeneity of peatland and tundra ecosystems. Recent approaches have used satellite-based land cover classifications, photosynthetic leaf area maps, or wetness indices to "up-scale" CO_2 (Forbrich et al., 2011; Marushchak et al., 2013) and CH_4 (Tagesson et al., 2013; Sturtevant and Oechel, 2013) flux measurements. Remote sensing inputs have also been used in conjunction with biophysical process modeling to estimate landscape-level changes in plant carbon assimilation and soil CO_2 emissions (Yuan et al., 2011; Tagesson et al., 2012a; Yi et al., 2013). Previous analyses of regional CH_4 emissions have ranged from the relatively simple modification of CH_4 emission rate estimates for wetland fractions according to temperature and carbon substrate constraints (Potter et al., 2006; Clark et al., 2011) or the use of more complex multi-layer wetland CH_4 models with integrated hydrological components (McGuire et al., 2012; Wania et al., 2013). Yet, most investigations have not examined the potential for simultaneously assessing CO_2 and CH_4 fluxes, and the corresponding net ecosystem carbon balance (NECB; Sitch et al., 2007; Olefeldt et al., 2012; McGuire et al., 2012) for peatland and tundra using a satellite remote sensing based model approach.

It is well recognized that sub-surface conditions influence the land-atmosphere exchange of CO_2 and CH_4 production. However, near-surface soil temperature, moisture and carbon substrate availability play a crucial role in regulating ecosystem carbon emissions. Strong associations between surface soil temperature (≤ 10 cm depth) and CO_2 respiration have been observed in Arctic peatland and tundra permafrost systems (Kutzbach et al., 2007). Significant relationships between CH_4 emissions and temperature have also been reported (Hargreaves et al., 2001; Zona et al., 2009; Sachs et al., 2010). Although warming generally increases the decomposition of organic carbon, the magnitude of CO_2 production is constrained by wet soil conditions (Olivas et al., 2010) which instead favor CH_4 emissions and decrease methantrophy in soil and litter layers (Turetsky et al., 2008; Olefeldt et al., 2012). Oxidation by methanotrophic communities in surface soils can reduce CH_4 emissions by over 90 % when gas transport occurs through diffusion (Preuss et al., 2013), but this constraint is often minimized when pore water content rises above 55–65 % (von Fischer and Hedin, 2007; Sjögersten and Wookey, 2009). Despite increases in the availability of organic carbon and accelerated CO_2 release due to increased soil temperature and thickening of the active layer in permafrost soils (Dorrepaal et al., 2009), anaerobic communities have shown a preference for light-carbon fractions (e.g. amines, carbonic acids) that are more abundant in the upper soil horizons (Wagner et al., 2009). Similarly, labile carbon substrates from recent photosynthesis and root exudates have been observed to increase CH_4 production relative to heavier organic carbon fractions (Ström et al., 2003; Dijkstra et al., 2012; Olefeldt et al., 2013).

The objective of this study was to evaluate the feasibility of using a satellite remote sensing data driven modeling approach to assess the daily and seasonal variability in CO_2 and CH_4 fluxes from northern peatland and tundra ecosystems, according to near-surface environmental controls including soil temperature, moisture and available soil organic carbon. In this paper we incorporate a newly developed CH_4 emissions algorithm within an existing Terrestrial Carbon Flux (TCF) CO_2 model framework (Kimball et al., 2012; Yi et al., 2013). The CH_4 emissions algorithm simulates gas production using near-surface temperature, anaerobic soil fractions and labile organic carbon as inputs. Plant CH_4 transport is determined by vegetation growth characteristics derived from gross primary production (GPP), plant functional traits and canopy/surface turbulence. Methane diffusion is determined based on temperature and moisture constraints to gas movement through the soil column, and oxidation potential. Ebullition of CH_4 is assessed using a simple gradient method (van Huissteden et al., 2006).

The integrated TCF model framework allows for satellite remote sensing information to be used as primary inputs and requires minimal parameterization relative to more complex ecosystem process models. It also provides an initial step towards the regional satellite-based monitoring of terrestrial CO_2 and CH_4 emissions, and the NECB, that will be capable of exploiting new spatially contiguous soil moisture and thermal data products to be produced under the upcoming NASA Soil Moisture Active Passive (SMAP) mission (Entekhabi et al., 2010). Although the NECB also encompasses

BGD
10, 16491–16549, 2013

other mechanisms of carbon transport, including dissolved and volatile organic carbon emissions and fire-based particulates, the NECB is limited in this study to terrestrial CO_2 and CH_4 fluxes, which often are primary contributors in high latitude tundra and peatland ecosystems (McGuire et al., 2010).

To evaluate the combined CO_2 and CH_4 algorithm approach, we compared TCF model simulations to tower EC records from six northern peatland and tundra sites within North America and Eurasia. For this study, baseline TCF simulations driven with tower EC based GPP and in-situ meteorology data were first used to assess the capability of the TCF model approach to quantify temporal changes in landscape scale carbon (CH_4 and CO_2) fluxes. Secondly, CO_2 and CH_4 simulations using internal TCF model GPP estimates (Yi et al., 2013) and inputs from satellite and global model reanalysis records were used to evaluate the relative uncertainty introduced when driving the model using coarser scale information in place of in-situ data. These satellite and reanalysis driven TCF simulations were then used to evaluate annual CO_2 and CH_4 fluxes at the six tower sites, and the relative impact of CH_4 emissions on the NECB.

2 Methods

2.1 TCF model description

The combined TCF CO_2 and CH_4 flux model framework regulates carbon gas exchange using soil surface temperature, moisture and soil organic carbon availability as inputs, and has the flexibility to run simulations at local and regional scales. TCF model estimates of ecosystem respiration (R_{eco}) and net ecosystem CO_2 exchange (NEE) at a daily time step have been evaluated against tower EC datasets from boreal and tundra systems using GPP, surface (≤ 10 cm depth) soil temperature (T_s) and volumetric moisture content (θ) inputs available from global model reanalysis and satellite remote sensing records (Kimball et al., 2009; McGuire et al., 2012). A recent adjustment to the TCF model (Kimball et al., 2012; Yi et al., 2013) incorporates a light-use efficiency

(LUE) algorithm that provides internally derived GPP calculations to determine R_{eco} and NEE fluxes. The adjusted TCF CO_2 model also allows for better user control over parameter settings and surface meteorological inputs (Kimball et al., 2012). The TCF CO_2 and newly added CH_4 flux model components are described in the following sections. A summary of the TCF model inputs, parameters, and the associated parameter values used in this study is provided in the Supplement (Tables S1 and S2; Fig. S1).

2.1.1 CO_2 flux component

The internal TCF LUE algorithm estimates daily GPP fluxes according to a biome-dependent vegetation maximum LUE coefficient (ε_{max}; $\mathrm{mg\,C\,MJ^{-1}}$) which represents the optimal conversion of absorbed solar energy and CO_2 to plant organic carbon through photosynthesis (Kimball et al., 2012). To account for environmental constraints on photosynthesis, ε_{max} is reduced (ε) using dimensionless linear rate scalars ranging from 0 (total inhibition) to 1 (no inhibition) that are described elsewhere (i.e. Kimball et al., 2012; Yi et al., 2013). Following the approach of Running et al. (2004), daily minimum air temperature (T_{min}) and atmospheric vapor pressure deficit (VPD) are used to define the environmental constraints on GPP. In this study we include a constraint based on θ to account for the sensitivity of bryophytes and shallow rooted species to surface drying (Wu et al., 2013), where θ_{min} and θ_{max} are specified minimum and maximum parameter values:

$$\varepsilon = \varepsilon_{max} \times f(\mathrm{VPD}) \times f(T_{min}) \times f(\theta) \qquad (1)$$
$$\text{where } f(\theta) = (\theta - \theta_{min})/(\theta_{max} - \theta_{min}).$$

Simulated GPP ($\mathrm{g\,C\,m^{-2}\,d^{-1}}$) is obtained as:

$$\mathrm{GPP} = \varepsilon \times 0.45\,\mathrm{SW_{rad}} \times \mathrm{FPAR} \qquad (2)$$

where $\mathrm{SW_{rad}}$ ($\mathrm{W\,m^{-2}}$) is incoming shortwave radiation and FPAR is the fraction of daily photosynthetically active solar radiation (PAR; $\mathrm{MJ\,m^{-2}}$) absorbed by plants during photosynthesis. For this approach, PAR is assumed to be 45 % of $\mathrm{SW_{rad}}$ (Zhao et al.,

BGD
10, 16491–16549, 2013
A satellite data driven biophysical modeling
J. D. Watts et al.

2005). Remotely sensed normalized difference vegetation index (NDVI) records have been used to estimate vegetation productivity (Schubert et al., 2010a; Parmentier et al., 2013) and changes in growing season length (Beck and Goetz, 2011) across northern peatland and tundra environments. Daily FPAR is derived using the approach of Badawy et al. (2013) to mitigate potential biases in low biomass landscapes (Peng et al., 2012):

$$\mathrm{FPAR} = \frac{0.94(\mathrm{Index} - \mathrm{Index}_{\mathrm{min}})}{\mathrm{Index}_{\mathrm{range}}} \tag{3}$$

This approach uses NDVI or simple ratio (SR; i.e. $(1+\mathrm{NDVI})/(1-\mathrm{NDVI})$) indices as input Index values. The results are then averaged to obtain FPAR. $\mathrm{Index}_{\mathrm{range}}$ corresponds to the difference between the 2nd and 98th percentiles in the NDVI and SR distributions (Badawy et al., 2013).

Biome-specific autotrophic respiration (R_a) is estimated using a carbon use efficiency (CUE) approach that considers the ratio of net primary production (NPP) to GPP (Choudhury, 2000). Carbon loss from heterotrophic respiration (R_h) is determined using a 3-pool soil litter decomposition scheme consisting of metabolic (C_{met}), structural (C_{str}) and recalcitrant (C_{rec}) organic carbon pools with variable decomposition rates. The C_{met} pool represents easily decomposable plant residue and root exudates including amino acids, sugars and simple polysaccharides, whereas the C_{str} pool consists of more recalcitrant litter residue such as hemi-cellulose and lignin (Ise et al., 2008; Porter et al., 2010). The C_{rec} pool includes physically and chemically stabilized carbon derived from the C_{met} and C_{str} pools and also corresponds to humified peat. A fraction of daily NPP (F_{met}) is first allocated as readily decomposable litterfall to C_{met} and the remaining portion ($1-F_{\mathrm{met}}$) is transferred to C_{str} (Ise and Moorcroft, 2006; Kimball et al., 2009). To account for reduced mineralization in tundra and peatland environments, approximately 70 % of C_{str} (F_{str}) is reallocated to C_{rec} (Ise and Moorcroft, 2006; Ise et al.,

BGD
10, 16491–16549, 2013

2008):

$$dC_{met}/dt = \text{NPP} \times F_{met} - R_{h,\,met} \tag{4}$$

$$dC_{str}/dt = \text{NPP}\,(1 - F_{met}) - (F_{str} \times C_{str}) - R_{h,\,str} \tag{5}$$

$$dC_{rec}/dt = (F_{str} \times C_{str}) - R_{h,\,rec} \tag{6}$$

CO_2 loss from $C_{met}(R_{h,\,met})$ is determined using an optimal decomposition rate parameter (K_p) that is attenuated (K_{met}) by dimensionless T_s and θ based multipliers (T_{mult} and W_{mult}, respectively) constrained between 0 and 1 to account for the reduced decomposition of soil organic carbon due to environmental conditions:

$$K_{met} = K_p \times T_{mult} \times W_{mult} \tag{7}$$

$$T_{mult} = \exp\left[308.56\left(66.02^{-1} - (T_s + T_{ref} - 66.17)^{-1}\right)\right] \tag{8}$$

$$W_{mult} = 1 - 2.2(\theta - \theta_{opt})^2 \tag{9}$$

The cold temperature constraints are imposed using an Arrhenius-type function (Lloyd and Taylor, 1994; Kimball et al., 2009) where decomposition is no longer limited when average daily T_s exceeds a user-specified reference temperature (T_{ref}; in K) which can vary with carbon substrate complexity, physical protection, oxygen availability and water stress (Davidson and Janssens, 2006). The W_{mult} modifier accounts for the inhibitory effect of dry and near-saturated soil moisture conditions on heterotrophic decomposition (Oberbauer et al., 1996). For this study, θ_{opt} is set to 80 % of pore saturation to account for ecosystem adaptations to wet soil conditions (Ise et al., 2008; Zona et al., 2012) and near-surface oxygen availability provided by plant root transport (Elberling et al., 2011). Decomposition rates for C_{str} and C_{rec} (K_{str}, K_{rec}) are determined as 40 % and 1 % of K_{met}, respectively (Kimball et al., 2009), and R_h is the total CO_2 loss from the three soil organic carbon pools:

$$R_h = K_{met} \times C_{met} + K_{str} \times C_{str} + K_{rec} \times C_{rec} \tag{10}$$

BGD
10, 16491–16549, 2013

Finally, the TCF model estimates NEE ($g\,C\,m^{-2}\,d^{-1}$) as the residual difference between R_{eco}, which includes R_a and R_h respiration components, and GPP. Negative (−) and positive (+) NEE fluxes denote respective terrestrial CO_2 sink and source activity:

$$\mathrm{NEE} = (R_a + R_h) - \mathrm{GPP} \tag{11}$$

2.1.2 CH_4 flux component

A CH_4 emissions algorithm was incorporated within the TCF model to estimate CH_4 fluxes for peatland and tundra landscapes. The modified TCF model estimates CH_4 production according to T_s, θ, and labile carbon availability. Plant CH_4 transport is modified by vegetation growth and production, plant functional traits, and canopy aerodynamic conductance which takes into account the influence of wind turbulence on moisture/gas flux between vegetation and the atmosphere. The TCF-CH_4 structure is similar to other process models (e.g. Walter and Heimann, 2000; van Huissteden et al., 2006) but reduces to a one-dimensional near-surface soil profile following Tian et al. (2010) to simplify model parameterization amenable to remote sensing applications. For the purposes of this study, the soil profile is defined for surface ($\leq 10\,cm$ depth) soil layers as most temperature and moisture retrievals from satellite remote sensing and reanalysis records do not characterize deeper soil conditions. Although this approach may not account for variability in carbon fluxes associated with deeper soil constraints, field studies from high latitude ecosystems have reported strong associations between CH_4 emissions and near-surface conditions including T_s and soil moisture (Hargreaves et al., 2001; Sachs et al., 2010; von Fischer et al., 2010; Sturtevant et al., 2012; Tagesson et al., 2012b).

CH_4 production

Soil moisture in the upper rhizosphere is a fundamental control on CH_4 production and emissions to the atmosphere. Methanogenesis (R_{CH_4}) within the saturated soil pore volume (ϕ_s; m^{-3}; aerated pore volume is denoted as ϕ_a) is determined according to an optimal CH_4 production rate (R_o; $\mu M\,CH_4\,d^{-1}$) and labile photosynthates:

$$R_{CH_4} = (R_o \times \phi_s) \times C_{met} \times Q_{10p}^{(T_s - T_p)/10} \tag{12}$$

For this study, CH_4 production was driven using the less recalcitrant C_{met} pool to reflect contributions by lower weight carbon substrates (Reiche et al., 2010; Corbett et al., 2012) in labile organic carbon-rich environments. Carbon contributions from the C_{str} pathway may also be allocated for CH_4 production in ecosystems with lower labile organic carbon inputs and higher contributions by hydrogenotrophic methanogenesis (Alstad and Whiticar, 2011). The Q_{10p} temperature modifier is used as an approximation to the Arrhenius equation and describes the temperature dependence of biological processes (Gedney and Cox, 2003; van Huissteden et al., 2006). The reference temperature (T_p) typically reflects mean annual or non-frozen season climatology. Both Q_{10p} and T_p can be adjusted, in addition to R_o, to accommodate varying temperature sensitivities in response to ecosystem differences in substrate quality and other environmental conditions (van Hulzen et al., 1999; Inglett et al., 2012). Methane additions from R_{CH_4} are first allocated to a temporary soil CH_4 storage pool (C_{CH_4}) prior to determining the CH_4 emissions for each 24 h time step; C_{met} is also updated to account for carbon losses due to CH_4 production.

CH_4 emission

The magnitude of daily CH_4 emissions (F_{total}) from the soil profile is determined through plant transport (F_{plant}), soil diffusion (F_{diff}) and ebullition (F_{ebull}) pathways:

$$F_{total} = F_{plant} + F_{diff} + F_{ebull} \tag{13}$$

Vegetation plays an important role in terrestrial CH_4 emissions by allowing for gas transport through the plant structure, avoiding slower diffusion through the soil column

BGD
10, 16491–16549, 2013

and often reducing the degree of CH_4 oxidation (Joabsson et al., 1999). Daily F_{plant} is determined using a rate constant (C_p) modified by vegetation growth and production (f_{grow}), an aerodynamic term (λ) and a rate scalar (P_{trans}) that account for differences in CH_4 transport ability according to plant functional type:

$$F_{\text{plant}} = (C_{CH_4} \times C_p \times f_{\text{grow}} \times \lambda \times P_{\text{trans}})(1 - P_{\text{ox}}) \quad (14)$$

A fraction of F_{plant} is oxidized (P_{ox}) prior to reaching the atmosphere and can be modified according to plant functional characteristics (Frenzel and Rudolph, 1998; Ström et al., 2005; Kip et al., 2010). Plant transport is further reduced under frozen surface conditions to account for pathway obstruction by ice and snow or bending of the plant stem following senescence (Hargreaves et al., 2001; Sun et al., 2012). The magnitude of f_{grow} is determined as the ratio of daily GPP to its annual maximum and is used to account for seasonal differences in root and above-ground biomass (Chanton, 2005).

Aerodynamic conductance (g_a) represents the influence of near-surface turbulence on energy/moisture fluxes between vegetation and the atmosphere (Roberts, 2000; Yan et al., 2012) and gas transport within the plant body (Sachs et al., 2008; Wegner et al., 2010; Sturtevant et al., 2012):

$$g_a = \frac{k^2 \mu_m}{\ln[(z_m - d)/z_{\text{om}}]\ln[(z_m - d)/z_{\text{ov}}]} \quad (15)$$

Values for z_m and d are the respective anemometer and zero plane displacement heights (m); z_{om} and z_{ov} are the corresponding roughness lengths (m) for momentum, heat and vapor transfer. The von Karman constant (k; 0.40) is a dimensionless constant in the logarithmic wind velocity profile (Högström, 1988), μ_m is average daily wind velocity (m s^{-1}), d is calculated as 2/3 of the vegetation canopy height, z_{om} is roughly 1/8th of canopy height (Yang and Friedl, 2002), and z_{ov} is 0.1 z_{om} (Yan et al., 2012). Estimated g_a is scaled between 0 and 1 to obtain λ using a linear function for sites with a lower observed sensitivity to surface turbulence. For environments with

BGD
10, 16491–16549, 2013

a higher sensitivity to surface turbulence, a quadratic approach is used when μ_m exceeds $4\,\mathrm{m\,s^{-1}}$:

$$\lambda = 0.0246 + 0.5091 g_a$$
$$\lambda = 0.0885 - (3.28 g_a) + \left(44.51 g_a^2\right), \mu_m > 4\,\mathrm{m\,s^{-1}} \tag{16}$$

Although this approach focuses on the influence of wind turbulence on plant gas transport within vegetated wetlands, it is also applicable for inundated microsites where increases in surface water mixing can stimulate CH_4 degassing (Sachs et al., 2010). In addition, Eq. (15) reflects near-neutral atmospheric stability and adjustments may be necessary to accommodate unstable or stable atmospheric conditions (Raupach, 1998).

The upward diffusion of CH_4 within the soil profile is determined using a one-layer approach similar to Tian et al. (2010). The rate of CH_4 transport (D_e; $\mathrm{m^{-2}\,d^{-1}}$) is considered for both saturated (D_{water}; $1.73 \times 10^{-4}\,\mathrm{\mu M\,CH_4\,d^{-1}}$) and aerated ($D_{air}$; $1.73\,\mathrm{\mu M\,CH_4\,d^{-1}}$) soil fractions:

$$D_e = (D_{water} \times \phi_s)(D_{air} \times \phi_a) \tag{17}$$

Potential daily transport through diffusion (P_{diff}) is estimated as the product of D_e and the gradient between C_{CH_4} and the atmospheric CH_4 concentration (Air_{CH_4}). This is further modified by soil tortuosity (τ; 0.66), which increases exponentially for $T_s < 274\,\mathrm{K}$ to account for slower gas movement at colder temperatures and barriers to diffusion resulting from near-surface ice formation (Walter and Heimann, 2000; Zhuang et al., 2004), and pathway constraints within the saturated pore fraction $(1-\theta)$:

$$P_{diff} = \tau \times D_e(C_{CH_4} - Air_{CH_4})(1-\theta)$$
$$T_s \geq 274, \quad \tau = 0.66 \tag{18}$$
$$T_s < 274, \quad \tau = 0.05 + 10^{-238} \times T_s^{97.2}$$

BGD
10, 16491–16549, 2013
A satellite data driven biophysical modeling
J. D. Watts et al.

A portion of diffused CH_4 is oxidized (R_{ox}) before reaching the soil surface, using a Michaelis–Menten kinetics approach scaled by ϕ_a:

$$R_{ox} = \frac{(V_{max} \times \phi_a)P_{diff}}{(K_m + \phi_a)P_{diff}} \times Q_{10d}^{(T_s - T_d)/10} \quad (19)$$

where V_{max} is the maximum reaction rate and K_m is the substrate concentration at 0.5 V_{max} (van Huissteden et al., 2006). Oxidation during soil diffusion is modified by soil temperature Q_{10} constraints (Q_{10d}); T_d is the reference temperature and can be defined using site-specific mean annual T_s (Le Mer and Roger, 2001). Total daily CH_4 emission (F_{diff}) from the soil diffusion pathway is determined by substracting R_{ox} from P_{diff}.

The TCF CH_4 algorithm uses a gradient-based approach to account for slow or "steady-rate" ebullition from inundated micro-sites in the landscape (Rosenberry et al., 2006; Wania et al., 2010), whereas episodic events originating deeper within the soil require more complex modeling techniques and input data requirements (Kettridge et al., 2011) that are beyond the scope of this study. Emission contributions due to ebullition occur when C_{CH_4} exceeds a threshold value (v_e) of 500 µM (van Huissteden et al., 2006). The magnitude of gas release is determined by steady-rate bubbling (C_e) applied within the saturated soil pore space (ϕ_s):

$$F_{ebull} = (C_e \times \phi_s)(C_{CH_4} - \upsilon_e),\ C_{CH_4} > v_e \quad (20)$$

2.2 Study sites and in-situ data records

Tower EC records from six peatland and tundra sites in Finland, Sweden, Russia, Greenland and Alaska were used to assess the integrated TCF CO_2 and CH_4 calculations (Fig. 1; Table 1). The Scandinavian tower sites include Siikaneva (SK) in southern Finland and Stordalen Mire (SM) in northern Sweden near the Abisko Scientific Research Station. The Lena River Delta (LR) site is located on Samoylov Island in northern Siberia and EC flux measurements from the Kytalyk (KY) flux tower were collected near Chokurdakh in northeastern Siberia. The Zackenberg (ZK) flux tower is located within Northeast Greenland National Park, and tower data records for Alaska were obtained from a water table manipulation experiment (Zona et al., 2009, 2012; Sturtevant et al., 2012) located approximately 6 km east of Barrow (BA). With exception of Siikaneva, the EC tower footprints represent wet permafrost ecosystems with complex, heterogeneous terrain that includes moist depressions, drier, elevated hummocks and inundated microsites. Vegetation within the tower footprints (Rinne et al., 2007; Riutta et al., 2007; Sachs et al., 2008; Jackowicz-Korczyński et al., 2010; Parmentier et al., 2011a; Zona et al., 2011; Tagesson et al., 2012b) consists of *Carex* and other sedges, dwarf shrubs (e.g. *Dryas* and *Salix*), grasses (e.g. *Arctagrostis*) and *Sphagnum* moss (with exception of Zackenberg).

For Siikaneva, T_s records from 5 and 10 cm depths were obtained for this analysis, but only water table depth information was available to describe soil wetness (Rinne et al., 2007). At the Lena River site T_s (5, 10 cm) and θ ($\leq$ 12 cm) observations were obtained from the nearby Samoylov meteorological station and represent tundra polygon wet center, dry rim and slope conditions (Boike et al., 2008; Sachs et al., 2008). Although θ was also measured during summer 2006 the records are limited to the wet polygon center location (J. Boike, personal communication, 2012) and were not used in this study due to the potential for overestimating saturated site conditions and corresponding CH_4 fluxes. For Zackenberg, in-situ T_s measurements were obtained for the 2 cm depth (Tagesson et al., 2012a, b) within the tower footprint; near-surface θ (< 20 cm) and 5 and 10 cm T_s measurements were collected adjacent to the site (Sigsgaard et al., 2011). At Stordalen Mire, in-situ θ was not available at the time of this study and T_s measurements were only for the 3 cm depth (Jackowicz-Korczyński et al., 2010). In-situ θ was also not collected at Kytalyk but T_s was obtained for the 4 cm depth for both low, wet and dry polygon locations, whereas T_s from the 8 cm depth was only available for the dry polygon (Parmentier et al., 2011a, b). The Barrow site includes southern, central and northern tower locations (Zona et al., 2009; Sturtevant et al., 2012). Soil T_s (5, 10 cm) and θ ($\leq$ 10 cm) information were collected at multiple locations within the Barrow tower footprints, but in 2009 T_s was only available at the 5 cm depth. For Barrow (2007), only CO_2 and CH_4 EC measurements corresponding to the north tower were used in the analysis, due to minimal EC data availability for the south and central tower sites following flux processing (Zona et al., 2009). Many of the Barrow CO_2 measurements were also rejected during data processing for the 2009 period; as a result NEE was not partitioned into R_{eco} and GPP (Sturtevant et al., 2012).

2.3 Remote sensing and reanalysis inputs

Daily input meteorology was obtained from the Goddard Earth Observing System Data Assimilation Version 5 (GEOS-5) MERRA archive (Rienecker et al., 2011) with $1/2 \times 2/3^{\circ}$ spatial resolution. The MERRA records were recently verified for terrestrial CO_2 applications in high latitude systems (Yi et al., 2011, 2013; Yuan et al., 2011), and provide model enhanced T_s and surface θ information similar to the products planned for the NASA SMAP mission (Kimball et al., 2012). In addition to near surface ($\leq$ 10 cm) T_s and θ information from the MERRA-Land reanalysis (Reichle et al., 2011) required for the R_{eco} and CH_4 simulations, daily MERRA SW_{rad}, T_{min} and VPD records were used to drive the internal TCF LUE model GPP calculations. The MERRA near-surface (2 m) wind parameters were also used to obtain mean daily μ_m for the CH_4 simulation estimates. The MERRA-Land records for Greenland are spatially limited due to land cover/ice masking inherent in the reanalysis product, and MERRA T_s and θ were not available for the Zackenberg tower site. As a proxy, T_s was derived from MERRA surface skin temperatures by applying a simple Crank–Nicholson heat diffusion scheme which accounts for energy attenuation with increasing soil depth (Wania et al., 2010); for θ, records from a nearby grid cell were used to represent moisture conditions at Zackenberg.

For the daily TCF LUE-based GPP simulations, quality screened cloud-filtered 16 day 250 m NDVI values from MODIS Terra (MOD13A1) and Aqua (MYD13Q1) data records (Solano et al., 2010) were obtained from the Oak Ridge National Laboratory Distributed Active Archive Center (ORNL DAAC). Differences between the MOD13A1 and

MYD13Q1 retrievals were minimal at the tower locations, and the combination of Terra and Aqua MODIS records reduced the retrieval gaps to approximate 8 day intervals. Linear interpolation was then used to scale the 8 day NDVI records to daily observations. The NDVI retrievals correspond to the center coordinate locations for each flux tower site. Coarser (500–1000 m resolution) NDVI records were not used in this study due to the close proximity of water bodies at the tower sites, which can substantially reduce associated FPAR retrievals. In addition, 250 m MODIS vegetation indices have been reported to better capture the overall seasonal variability in tower EC flux records (Schubert et al., 2012).

2.4 TCF model parameterization

A summary of the site specific TCF model parameters is provided in the Supplement (Table S2). Parameter values associated with grassland biomes were selected for the LUE model VPD and T_{min} modifiers used to estimate GPP (Yi et al., 2013), as more specific values for tundra and moss-dominated wetlands were not available. Parameter values for θ_{max} were obtained using growing-season maximum θ measurements for each site and θ_{min} was set to 0.15 for scaling purposes. Model ε_{max} was specified as 0.82 mg C MJ^{-1} for the duration of the growing season, although actual LUE can vary throughout the summer due to differences in vegetation growth phenology and nutrient availability (Connolly et al., 2009; King et al., 2011). Tundra CUE ranged from 0.45 to 0.55 (Choudhury, 2000); a lower CUE value of 0.35 was used for the moss-dominated Siikaneva tower site due to a more moderate degree of carbon assimilation occurring in bryophytes, that has been observed in other sub-Arctic communities (Street et al., 2012). For the TCF model F_{met} parameter, the percentage of NPP allocated to C_{met} varied between 70 and 72 % for tower tundra sites (Kimball et al., 2009) compared to 50 and 65 % for Siikaneva and Stordalen Mire where moss cover is more abundant. The TCF CH_4 module R_o parameter ranged from 4.5 and 22.4 µM CH_4 d^{-1} (Walter and Heimann, 2000; van Huissteden et al., 2006). Values for Q_{10p} varied between 3.5 and 4 due to enhanced microbial response to temperature variability under colder climate

BGD
10, 16491–16549, 2013

conditions (Gedney and Cox, 2003; Inglett et al., 2012). A Q_{10d} of 2 was assigned for CH_4 oxidation (Zhuang et al., 2004; van Huissteden et al., 2006). Parameter values for P_{trans}, which indicates relative plant transport ability, ranged from 7 to 9 (dimensionless); lower values were assigned to tower locations with a higher proportion of shrub and moss cover, whereas higher P_{trans} corresponds to sites where sedges are more prevalent (Ström et al., 2005; Rinne et al., 2007). For λ, the scaled conductance for lower site wind sensitivity was used for the CH_4 simulations, with exception of Lena River which showed a higher sensitivity to surface turbulence. Values for P_{ox} ranged from 0.7 in tundra to 0.8 in *Sphagnum*-dominated systems to account for higher CH_4 oxidation by peat mosses (Parmentier et al., 2011c). Due to a lack of detailed soil profile descriptions and heterogeneous tower footprints, soil porosity was assigned at 75 % for sites with more abundant fibrous surface layer peat (i.e. Siikaneva and Stordalen Mire) and 70 % elsewhere to reflect more humified or mixed organic and mineral surface soils (Elberling et al., 2008; Verry et al., 2011).

2.5 TCF model simulations

The TCF model was first evaluated against the tower EC records using simulations driven with in-situ measurement data including EC-based GPP, T_s, θ and μ_m inputs. This step allowed for baseline TCF model R_{eco} and CH_4 flux estimates to be assessed without introducing additional input uncertainties from the coarser reanalysis meteorology records and TCF LUE model-derived GPP calculations. Site mean daily T_s and θ measurement records corresponding to near-surface (≤ 10 cm) soil depths were used for the TCF site based model simulations when possible, to better coincide with the soil penetration depths anticipated for upcoming satellite-based microwave remote sensing missions (Kimball et al., 2012). In addition to the TCF model runs using site in-situ information, changes in temporal agreement and model uncertainty were evaluated for simulations where MERRA based θ, T_s, μ_m, or TCF LUE GPP inputs were used in place of the in-situ data. A final TCF model simulation included only input data from MODIS and MERRA and was used to establish annual GPP, R_{eco} and CH_4 carbon budgets for each site. Baseline carbon pools were initialized for each site by continuously cycling ("spinning-up") the TCF model for the tower years of record (described in Table 1) to reach a dynamic steady-state between estimated NPP and surface soil organic carbon stocks (Kimball et al., 2009). In-situ data records were used during the model spin-up to establish baseline organic carbon conditions for the first five TCF simulations, although it was often necessary to supplement these data with MERRA based information to obtain continuous annual time series. For the final model run, only MODIS and MERRA inputs were used during the spin-up process.

The temporal agreement between the tower EC records and TCF model simulations was assessed using Pearson correlation coefficients (r; ± one standard deviation) for the daily, 8 day, and total-period (EC length of record) cumulative carbon fluxes and corresponding tests of significance at a 0.05 probability level. The 8 day and total-period cumulative fluxes were evaluated, in addition to the daily fluxes, to account for differences between the TCF model estimates and tower EC records stemming from temporal lags between changing environmental conditions and resulting carbon (CO_2, CH_4) emissions (Lund et al., 2010; Levy et al., 2012). The mean residual error (MRE) between the tower EC records and TCF modeled CO_2 and CH_4 fluxes was used to identify potential model biases; root-mean-square-error (RMSE) differences were used as a measure of model estimate uncertainty in relation to the tower EC records.

3 Results

3.1 Surface organic carbon pools

The TCF model-generated surface soil organic carbon pools represent steady-state conditions obtained through the continuous cycling of in-situ or MODIS and MERRA environmental inputs for the years of record associated with each tower site (described in Table 1). Approximately 600 and 1000 yr of spin-up by the TCF model were required for the recalcitrant surface soil organic carbon pool to reach dynamic steady-state conditions at the peatland and tundra sites, respectively, which is similar to previous simulations conducted for northern EC tower locations (Kimball et al., 2009). The TCF model organic carbon pools are also comparable to northern soil carbon inventory records (Yi et al., 2013). Over 95 % of the resulting soil organic carbon pool was allocated to C_{rec} by the TCF model, with 2 to 3 % stored as C_{met} and the remainder partitioned to C_{str}. The estimated surface soil organic carbon pools from the in-situ based TCF model spin-up ranged from $\simeq 3.3\,kg\,C\,m^{-2}$ for Zackenberg and Stordalen Mire and 1.1 to $1.5\,kg\,C\,m^{-2}$ for the other tower sites. The larger organic carbon stocks at Zackenberg reflect a combination of relatively high tower EC based GPP inputs, often exceeding $5\,g\,C\,m^{-2}\,d^{-1}$ during the peak growth season, and a relatively short < 50 day peak growing season (Tagesson et al., 2012a) that minimized TCF modeled R_h losses. Although it was necessary to use internal LUE based GPP calculations for Stordalen Mire in the absence of available CO_2 records, the resulting TCF based C_{met} and C_{rec} carbon stocks were similar in magnitude to plant litter measurements collected at this site (Olsrud and Christensen, 2011). However, the TCF simulated soil organic carbon stock for Lena River was less than the $2.9\,kg\,C\,m^{-2}$ average determined from in-situ samples (≤ 10 cm depth) collected from nearby river terrace soils (Zubrzycki et al., 2013), possibly due to spatial heterogeneity or the use of recent climate records for model spin-up that may not adequately reflect past site conditions. The influence of input GPP and temperature conditions on the TCF model soil organic carbon pools was also observed in results from the MODIS and MERRA driven spin-up, where the total soil organic carbon estimates increased by 164 % on average for the Siikaneva, Lena River, Kytalyk and Barrow tower sites. This increase resulted primarily from significantly ($p < 0.05$) cooler (0.1 to 4 °C) MERRA T_s conditions and higher LUE based GPP inputs (by approximately 13 %). In contrast, a decrease in surface soil organic carbon stocks for Zackenberg (47 %) and Stordalen Mire (11 %) resulted from significantly ($p < 0.05$) lower LUE modeled GPP by roughly 14 % and warmer (2.3 °C, on average) input MERRA T_s, respectively.

BGD
10, 16491–16549, 2013

3.2 LUE based GPP

The TCF LUE model GPP simulations derived using MODIS and MERRA inputs captured the overall seasonality observed in the tower EC records (Fig. 2) and explained 76 % (r^2; $p < 0.05$, $N = 7$) of variability in the total EC period-of-record fluxes (Fig. 3). While correspondence between the tower EC and TCF GPP estimates was also strong ($r^2 = 75 \pm 16$ %) for the 8 day cumulative fluxes, model-tower agreement decreased considerably for daily GPP ($r^2 = 57 \pm 22$ %). The lower daily correspondence partially reflects a delayed response in vegetation productivity and growth following changes in atmospheric and soil conditions (Lund et al., 2010) that was not adequately represented in the LUE model. Temporal fluctuations in MERRA SW_{rad} also contributed to short-term increases in TCF simulated GPP that were not always observed in the tower EC records. In addition, an insufficient representation of seasonal phenology by the TCF LUE model may have contributed to differences between the tower and TCF GPP fluxes. This was most apparent for the Barrow and Kytalyk sites where the TCF results overestimated the tower GPP fluxes towards the start of growing season (Fig. 2). The large increase in TCF GPP at Kytalyk from 8–30 June (DOY 159–181) resulted from a short-term warming event observed in both the MERRA reanalysis and local tower temperature measurements that was not reflected in the EC GPP estimates. To examine the possibility that a shallow (< 14 cm) early season thaw depth within the Kytalyk tower footprint may have reduced the degree of vegetation response to short-term warming, particularly for deeper rooting *Betula nana* and *Salix pulchra*, an additional simulation was conducted using the temperature driven bud break phenology model described in Parmentier et al. (2011a) to determine the start of LUE derived GPP activity. This step reduced the corresponding TCF and tower GPP RMSE difference for Kytalyk by 56 %, from 2.2 to approximately 1 $g\,C\,m^{-2}\,d^{-1}$ with an associated r^2 of 67 %.

Although previous LUE models (e.g. Running et al., 2004; Yi et al., 2013) have relied solely on VPD to represent water related constraints to GPP, the approach used in this investigation included an additional soil moisture component to better account for bryophyte sensitivity to surface drying (Wu et al., 2013). The additional θ constraint reduced the overall TCF and tower GPP RMSE (1.3 vs. 1.5 $\mathrm{g\,C\,m^{-2}\,d^{-1}}$) and MRE (−0.1 vs. −0.8 $\mathrm{g\,C\,m^{-2}\,d^{-1}}$) differences by approximately 14 and 92 %. However, the TCF simulations continued to overestimate the EC based GPP fluxes for Siikaneva, Lena River in 2003, and Kytalyk (MRE = $-0.6 \pm 0.8\,\mathrm{g\,C\,m^{-2}\,d^{-1}}$), and slightly underestimated GPP elsewhere (MRE = $0.3 \pm 0.3\,\mathrm{g\,C\,m^{-2}\,d^{-1}}$). This variability in model GPP bias could be influenced by inconsistencies between the coarse scale MERRA inputs and local tower meteorology, which have also been reported elsewhere (i.e. Yi et al., 2013). For instance, periods of warmer (3 to 4 °C) MERRA T_{min} inputs relative to local measurements for the Lena River site in 2003 resulted in seasonally higher model GPP fluxes. In contrast, mid-summer MERRA T_{min} for the Barrow northern tower site in 2007 was 2 to 7 °C cooler than the local tower meteorology and led to significantly lower ($p < 0.05$) model GPP estimates. Some of the observed biases between the TCF derived and site GPP estimates could also be due to site-specific differences in the light response curve and respiration model parameterizations (i.e. Aurela et al., 2007; Kutzbach et al., 2007; Parmentier et al., 2011a; Tagesson et al., 2012; Zona et al., 2012) used when partitioning the EC NEE fluxes into GPP and R_{eco}. However, it is difficult to quantify the extent to which discrepancies between the TCF and EC derived GPP estimates can be directly attributed to the flux partitioning routines.

3.3 R_{eco} and NEE

The TCF model R_{eco} simulations derived using local tower inputs accounted for 59 ± 28 % and 76 ± 24 % (r^2) of variability in respective daily and 8 day cumulative tower EC fluxes (Fig. 4). As observed with GPP, the correspondence between the in-situ TCF model R_{eco} results and tower EC records increased to 89 % (r^2; $p < 0.05$, $N = 6$) when considering total-period cumulative fluxes (Fig. 3). The RMSE differences between the in-situ TCF R_{eco} and tower EC records varied considerably (0.3 to 1.3 $\mathrm{g\,C\,m^{-2}\,d^{-1}}$), but the lowest model errors were observed for the permafrost-free Siikaneva fen site (Table 2). The in-situ TCF results underestimated tower R_{eco} ($0.1 \leq \mathrm{MRE} \leq 0.3\,\mathrm{g\,C\,m^{-2}\,d^{-1}}$)

for the Siikaneva, Lena River (2006) and Zackenberg sites and overestimated tower R_{eco} ($-1 \leq \mathrm{MRE} \leq -0.1\,\mathrm{g\,C\,m^{-2}\,d^{-1}}$) elsewhere. Additional TCF simulations were conducted for selected tower sites having 10 cm depth T_s records to examine the potential influences of colder sub-surface T_s conditions on model R_{eco} activity that were not accounted for by the shallow ($\leq$ 5 cm in-situ depth) temperature inputs (Parmentier et al., 2011a). These simulations reduced overall RMSE differences between the in-situ TCF and tower R_{eco} estimates (reported in Table 2) by approximately 12 %. The TCF NEE estimates derived from local tower observations explained approximately 75 ± 12 % and 81 ± 11 % (r^2) of respective daily and 8 day cumulative variability in the tower EC records (Table 2). The r^2 correspondence between the in-situ TCF model NEE and total period-of-record tower fluxes was also 75 % ($p \leq 0.05$) when excluding the Kytalyk site, for which the TCF estimates were exceptionally low relative to the EC observed NEE sink (−16.3 vs. $-81.8\,\mathrm{g\,C\,m^{-2}}$). The overall RMSE and MRE differences between the in-situ TCF and tower NEE records were $0.7 \pm 0.4\,\mathrm{g\,C\,m^{-2}\,d^{-1}}$ and $0.1 \pm 0.4\,\mathrm{g\,C\,m^{-2}\,d^{-1}}$ respectively.

The TCF R_{eco} results derived using coarser MODIS and MERRA inputs accounted for 51 ± 29 % and 71 ± 17 % (r^2) of variability in respective daily and 8 day tower EC records (Fig. 4; Table 2). However, only 44 % of the variability in the total period-of-record R_{eco} fluxes was explained by the MODIS and MERRA based TCF simulations (Fig. 3) due to higher (by approximately 170 %) model R_{eco} predictions for Kytalyk and Lena River (2003). The RMSE and MRE differences between the MODIS and MERRA driven TCF and tower R_{eco} estimates were 0.9 ± 0.4 and $-0.2 \pm 0.9\,\mathrm{g\,C\,m^{-2}\,d^{-1}}$, respectively. Using the internal TCF model GPP estimates increased the overall model and tower RMSE differences for R_{eco} by 23 % relative to the in-situ TCF results, compared to a respective 3 and 14 % increase when incorporating MERRA θ or T_s inputs (Fig. 5). Tower and TCF correspondence for R_{eco} at the respective daily and 8 day time steps was also lower (r^2 = 32 % and 56 %) for simulations using the internal TCF GPP estimates, relative to those derived using MERRA θ or T_s inputs (r^2 = 57 % and 72 %).

BGD
10, 16491–16549, 2013

The model and tower NEE correspondence derived using the MODIS and MERRA TCF inputs was strong at the 8 day time step ($r^2 \geq 85\,\%$) for Siikaneva, Lena River (2003) and Zackenberg (2009) compared to lower correspondence ($r^2 \leq 45\,\%$) for the other site records (Table 2). The relationship between the tower NEE records and MODIS and MERRA based TCF results was not significant for Kytalyk and the northern Barrow site in 2007 ($r \leq 0.20$; $p \geq 0.16$). Overall, the TCF NEE results derived using MERRA θ and T_s inputs explained approximately 56 % and 72 % (r^2) of the respective daily and 8 day cumulative variability in the tower EC fluxes (Fig. 5). This decreased to 32 % (daily) and 56 % (8 day cumulative), respectively, when substituting the internal TCF LUE estimates for the input tower GPP records. Similar decreases in temporal correspondence between model derived carbon fluxes and wetland EC observations have been reported elsewhere (Zhang et al., 2012b) and are often influenced by temporal lags between fluctuating environmental conditions and carbon emissions (Levy et al., 2012). The RMSE difference between the MODIS and MERRA TCF based NEE simulations and the tower EC records averaged 1 (±0.5) $g\,C\,m^{-2}\,d^{-1}$, which is similar to the results from previous TCF based studies using coarse resolution satellite remote sensing and reanalysis information (Yi et al., 2013). As observed with the in-situ based TCF model results, the largest difference in total record-period NEE occurred for Kytalyk where the MODIS and MERRA based TCF simulations indicated only a small net carbon gain ($-24.7\,g\,C\,m^{-2}$) relative to the tower EC record ($-82.4\,g\,C\,m^{-2}$; Fig. 3). An overall positive bias in the TCF model NEE fluxes ($\text{MRE} = 0.3 \pm 0.5\,g\,C\,m^{-2}\,d^{-1}$) was observed in the MODIS and MERRA TCF based simulation results (Table 2), but decreased to $0.1 \pm 0.2\,g\,C\,m^{-2}\,d^{-1}$ when excluding the less favorable Kytalyk and Barrow northern record estimates ($\text{MRE} \geq 0.9\,g\,C\,m^{-2}\,d^{-1}$).

3.4 CH_4 fluxes

The TCF model CH_4 simulations derived using local tower inputs accounted for $64 \pm 11\,\%$ (excluding Kytalyk; $p = 0.10$) and $80 \pm 12\,\%$ (r^2) of respective variability in the daily and 8 day tower fluxes (Fig. 6; Table 3). The TCF results are similar to CH_4 flux estimates for these sites that were obtained using more complex biogeochemical models (e.g. Wania et al., 2010; Zhang et al., 2012b; Zürcher et al., 2013). The r^2 correspondence between the in-situ TCF simulations and tower CH_4 fluxes increased to 98 % when considering total period-of-record emissions across all sites (Fig. 3; $p < 0.05$, $N = 9$). For the Kytalyk site, Parmentier et al. (2011b) reported large differences in EC half-hourly CH_4 fluxes due to short term changes in wind direction. Larger CH_4 emissions were often observed when the EC fluxes represented upwind portions of the tower footprint containing inundated microsites or plant communities such as *Carex* sp. and *E. angustifolium*. Although this short-term variability in CH_4 fluxes may have contributed to the observed discrepancy between the TCF and EC based emission estimates, attempts to systematically screen the EC observations based on wind direction, or to use daily EC medians instead of mean values, did not substantially improve the model results.

The RMSE differences between the local TCF CH_4 fluxes and tower records varied from 6.7 to 42.5 $\mathrm{mg\,C\,m^{-2}\,d^{-1}}$. The local TCF simulations over predicted the EC tower CH_4 fluxes ($-12.6 \leq \mathrm{MRE} \leq -1.2$ $\mathrm{mgC\ m^{-2}\,d^{-1}}$) for the Siikaneva, Lena River 2006, Zackenberg 2009, and Barrow 2009 north and central tower records, and underestimated tower CH_4 fluxes ($0.5 \leq \mathrm{MRE} \leq 6.3\,\mathrm{mg\,C\,m^{-2}\,d^{-1}}$) elsewhere. Incorporating μ_m as an additional TCF CH_4 model constraint better elucidated the temporal variability in CH_4 emissions influenced by localized changes in gas flow between vegetation and the atmosphere (Grosse et al., 1996; Joabsson et al., 1999). Without including μ_m in the model, the mean daily correspondence between the tower EC and TCF CH_4 fluxes decreased to $r^2 < 40\,\%$ and RMSE increased by > 10 %. The most substantial difference in the TCF model results was observed for Lena River, where excluding the μ_m modifier reduced the daily and 8 day emissions correspondence by over 60 %. The μ_m modifier also improved the TCF model characterization of emissions activity at Zackenberg in late autumn where wind turbulence has been reported to increase CH_4 fluxes following soil freeze events, by driving gas transfer through plant aerenchyma and moss surface layers (Tagesson et al., 2012b).

Unlike the TCF R_{eco} results, using deeper (10 cm depth) T_s measurement inputs did not improve the model RMSE values, except for Barrow north in 2007 where the RMSE decreased by 35 %. This contradictory response may reflect methanogen sensitivity to changing deeper (≤ 15 cm) T_s following site water table manipulations that increased the active layer depth (Zona et al., 2009, 2012). In contrast, the model RMSE for Lena River was 15 % higher when using in-situ 10 cm T_s records in the TCF model simulations instead of the 5 cm depth measurements. A 6 % improvement in model RMSE also occurred when using the 3 to 5 °C warmer 2 cm T_s records for Zackenberg 2008, which resulted in higher (by 12 %; 0.5 g C m^{-2}) summer TCF CH_4 estimates relative to model simulations using 5 cm T_s. Contrary to expectations, the 2 cm T_s measurements did not improve the model RMSE for Zackenberg 2009. This difference may have been influenced by relatively warmer and wetter site conditions in 2008 compared to 2009 (Tagesson et al., 2012a); CH_4 fluxes in wet or inundated Arctic landscapes are reportedly more sensitive to changes in T_s compared to those with drier surface soils (Olefeldt et al., 2013). Seasonal variability in environmental conditions, including carbon substrate availability, may also lead to differences in methanogen response to T_s within the soil profile. For example, Rinne et al. (2007) reported that T_s from the 35 cm depth best explained CH_4 emissions from Siikaneva in 2005. In contrast, using these T_s measurements to drive the TCF model resulted in underestimation of CH_4 fluxes prior to mid-summer and substantially reduced the overall correspondence between the model simulations and EC records.

The TCF CH_4 simulations derived from MODIS and MERRA inputs (Fig. 5; Table 3) accounted for 48 ± 16 % and 79 % ± 8 % (r^2, $p < 0.05$) of respective daily and 8 day variability in the tower EC records when excluding the less favorable results for Kytalyk (r^2 = 8 and 44 %, respectively). Although slightly lower than the local TCF CH_4 estimates, the MODIS and MERRA driven simulations explained 96 % (r^2) of tower observed variability in the total period-of-record CH_4 fluxes across all sites (Fig. 3). The corresponding RMSE and MRE differences between the tower and TCF CH_4 records were 18.2 ± 13.6 and 1.8 ± 7.3 mg C m^{-2} d^{-1} respectively. Replacing the site records with the internal TCF GPP estimates or MERRA reanalysis information in the TCF simulations increased the overall model RMSE by only 13 % (Fig. 7) relative to the in-situ based results. Although the agreement between daily TCF and tower CH_4 fluxes was low (r^2 = 35 %) when incorporating MERRA μ_m (Fig. 7) relative to the other model simulation results ($r^2 < 50$ %), this was primarily due to an inability of the reanalysis μ_m data to capture changes in anemometer-observed mean daily wind velocity at the Lena River and Kytalyk tower sites.

3.5 Estimates of annual carbon budgets

The MODIS and MERRA based TCF simulations indicated a net CO_2 sink (NEE = −34.5 ± 18.5 $\mathrm{g\,C\,m^{-2}\,yr^{-1}}$) for the tower sites, excluding Barrow in 2009 (NEE = 7.3 $\mathrm{g\,C\,m^{-2}\,yr^{-1}}$) where the estimated R_{eco} emissions exceeded annual GPP (Fig. 8). Other studies near Barrow have also reported NEE losses from wet tundra communities, resulting from a combination of variable soil wetness and warming which can strongly influence R_{eco} (Huemmrich et al., 2010b; Sturtevant and Oechel, 2013). The corresponding TCF R_{eco} estimates ranged from 133 (Zackenberg in 2009) to 494 $\mathrm{g\,C\,m^{-2}\,yr^{-1}}$(Stordalen Mire in 2006) with lower CO_2 emissions occurring in the colder, more northern tundra sites (Fig. 8). The strongest NEE carbon sink indicated by the MODIS and MERRA based TCF simulations was observed for the peat-rich Siikaneva site (−70.3 $\mathrm{g\,C\,m^{-2}\,yr^{-1}}$) due to high annual GPP (462.5 $\mathrm{g\,C\,m^{-2}\,yr^{-1}}$) relative to the other tower locations. Although tower EC records for CO_2 were not available for Stordalen Mire in 2006 and 2007 to verify the TCF NEE results (−50.8 and −65.8 $\mathrm{g\,C\,m^{-2}\,yr^{-1}}$, respectively), the TCF model NEE estimates are slightly smaller (∼ 30 $\mathrm{g\,C\,m^{-2}\,d^{-1}}$) than other estimates of annual carbon exchange for this time period (Christensen et al., 2012) but are similar to values reported for other years at this site (Olefeldt et al., 2012; Marushchak et al., 2013).

The TCF CH_4 annual flux estimates determined using MODIS and MERRA inputs averaged 6.9 (±5.5) $\mathrm{g\,C\,m^{-2}\,yr^{-1}}$ for the six tower sites. The highest CH_4 emissions

BGD
10, 16491–16549, 2013

were observed for Stordalen Mire and Siikaneva ($\geq 11.8\ \mathrm{g\,C\,m^{-2}\,yr^{-1}}$), due to higher model-defined CH_4 production rates in combination with MERRA summer T_s records that were often 5 °C warmer than the other sites. In contrast to the other tower locations, model CH_4 emissions were lowest for Barrow in 2007 ($1.8\ \mathrm{g\,C\,m^{-2}\,yr^{-1}}$) due to more minimal TCF GPP estimates and colder mean MERRA daily summer T_s conditions that did not reflect the abnormally warm site conditions that occurred during this year (Shiklomanov et al., 2010). The TCF annual CH_4 emissions for Lena River in 2003 and 2006 were relatively small (2.6 and $2\ \mathrm{g\,C\,m^{-2}\,yr^{-1}}$, respectfully), but are similar in magnitude to an area-weighted CH_4 estimate for this site determined from coupled biogeochemical and permafrost models (Zhang et al., 2012b).

The TCF CH_4 fluxes contributed to only 1 to 5 % of annual carbon emissions ($R_{eco} + CH_4$) for the tower sites, which is similar to previous reports (Schneider von Deimling et al., 2012), but reduced the net ecosystem carbon balance ($-23.3 \pm 19.6\ \mathrm{g\,C\,m^{-2}\,yr^{-1}}$) by approximately 23 % relative to NEE. The annual TCF estimates indicated that the site CO_2 and CH_4 fluxes, excluding Barrow and Lena River, contributed to a net global warming potential (GWP) of $188 \pm 68\ \mathrm{g\,CO_2eq\,m^{-2}\,yr^{-1}}$ over a 100 yr time horizon (Boucher et al., 2009) with the total GWP influences by CH_4 at approximately 9 to 44 % that of R_{eco}. Similarly the Lena River and Barrow sites mitigated the GWP at a mean rate of $-40\ \mathrm{g\,CO_2eq\,m^{-2}\,yr^{-1}}$ in 2006 and 2007, but were net GWP contributors in 2003 and 2009 (at 25 and $160\ \mathrm{g\,CO_2eq\,m^{-2}\,yr^{-1}}$, respectfully). Although site CO_2 contributions from methantrophy during plant transport and soil diffusion were estimated to range from 3.8 to $58.3\ \mathrm{g\,C\,m^{-2}\,yr^{-1}}$, these contributions represented < 14 % of total TCF derived R_{eco}.

4 Discussion and conclusions

The level of complexity in biophysical process models has increased considerably in recent years but there remain large differences in carbon flux estimates for northern high latitude systems (McGuire et al., 2012; Wania et al., 2013). An integrated TCF CO_2 and CH_4 framework was developed to improve carbon model compatibility with remote sensing retrievals that can be used to inform changes in surface conditions across northern peatland and tundra regions. Although the TCF model lacks the biophysical and hydrologic complexity found in more sophisticated process models (e.g. Zhuang et al., 2004; Wania et al., 2010), it avoids the need for extensive parameterization by instead employing generalized surface vegetation growth, temperature, and moisture constraints on ecosystem CO_2 and CH_4 fluxes. Despite the relatively simple model approach and landscape heterogeneity at the tower sites, the TCF simulations derived from local tower inputs captured the overall seasonality and magnitude of R_{eco} and CH_4 fluxes observed in the tower EC records. Overall the TCF R_{eco}, NEE and CH_4 emissions determined from local site inputs showed strong mean correspondence (8 day $r > 0.80$; $p < 0.05$) with the tower EC records but the strength of agreement varied considerably for the daily fluxes due to temporal lags between changing environmental conditions and carbon emissions to the atmosphere (Zhang et al., 2012b) and larger EC uncertainty at the daily time step (Baldocchi et al., 2008; Yi et al., 2013). The RMSE for the local TCF R_{eco} and CH_4 fluxes averaged $0.7 \pm 0.4\,\mathrm{g\,C\,m^{-2}\,d^{-1}}$ and $17.9 \pm 11.5\,\mathrm{mg\,C\,m^{-2}\,d^{-1}}$ which is comparable to other site based model results (e.g. Marushchak et al., 2013; Sturtevant and Oechel, 2013).

We used near-surface T_s records in the TCF simulations to better coincide with the soil depths represented by existing reanalysis datasets and upcoming satellite remote sensing missions, but acknowledge that deeper T_s controls are also important for regulating high latitude carbon emissions. This was evident in TCF R_{eco} results where the RMSE differences between the site based TCF results and tower EC fluxes generally improved when using deeper 10 cm T_s inputs instead of those from shallower ($\leq$ 5 cm) soil depths. However, the TCF CH_4 simulations were more favorable when using near-surface (2 to 5 cm) T_s inputs. The observed CH_4 emission sensitivity to near-surface soil warming may be influenced by cold temperature constraints on CH_4 production in the carbon-rich root zone where organic acids are more abundant (Turet-

BGD
10, 16491–16549, 2013

sky et al., 2008; Olefeldt et al., 2013). Light-weight carbon fractions have been shown to be more susceptible to mineralization following soil thaw and temperature changes than the heavier, more recalcitrant soil organic carbon pools in high latitude environments (Glanville et al., 2012). However, it is also recognized that the depletion of older soil organic carbon stocks may become more prevalent in permafrost soils subject to thaw and physiochemical destabilization (Schuur et al., 2009; Hicks Pries et al., 2013a) in absence of wet, anoxic conditions (Hugelius et al., 2012; Hicks Pries et al., 2013b). Seasonal changes in T_s constraints were also evident in this study, especially in the Zackenberg records where the TCF model underestimated tower R_{eco} and CH_4 emissions in autumn by not accounting for warmer temperatures deeper in the active layer, which can sustain microbial activity following surface freezing (Aurela et al., 2002). Allowing the TCF model vegetation CUE parameter to change over the growing season instead of allocating R_a as a static fraction of GPP may also improve model and tower R_{eco} agreement. In Arctic tundra, R_a can contribute anywhere from 40 to 70 % of R_{eco}, with higher R_a occurring later in the growing season when root systems expand deeper into the active layer (Hicks Pries et al., 2013a). Representing R_a as a fixed proportion of daily GPP in the TCF model, and not accounting for the use of stored plant carbon reserves, may also have contributed to the lower R_{eco} estimates during spring and autumn transitional periods, when photosynthesis is reduced.

In this study we estimated peatland and tundra CO_2 fluxes using TCF model simulations driven by MERRA reanalysis and MODIS satellite remote sensing inputs and obtained respective RMSE differences from tower EC based observations of 1.3 ± 0.5 (GPP), 0.9 ± 0.4 (R_{eco}) and 1 ± 0.5 (NEE) $g\,C\,m^{-2}\,d^{-1}$. The resulting TCF model accuracy is similar to a previous TCF model analysis for the boreal and tundra regions (Yi et al., 2013), and other Arctic LUE based GPP studies (Tagesson et al., 2012a; McCallum et al., 2013). The model and tower RMSE for the MODIS and MERRA based CH_4 simulations was $18.2 \pm 13.6\,mg\,C\,m^{-2}\,d^{-1}$ and is also comparable to results from previous remote sensing based CH_4 studies (Meng et al., 2012; Tagesson et al., 2013). However, the MERRA reanalysis inputs used in this analysis are relatively coarse

BGD
10, 16491–16549, 2013

Title Page
Abstract Introduction
Conclusions References
Tables Figures
◂ ▸
Back Close
Full Screen / Esc
Printer-friendly Version
Interactive Discussion

$(1/2^{\circ} \times 2/3^{\circ})$ and may not fully reflect local climate and landscape variability within northern peatland and tundra systems, where large differences in surface T_s and moisture often occur in close proximity (Sachs et al., 2008; Sturtevant et al., 2012). Further improvement in the TCF LUE model is also needed to better capture temporal changes in GPP during spring and autumn transitional periods and to improve associated residual NEE estimates for peatland and tundra. This was observed in the lower mean 8 day correspondence ($p < 0.05$) for GPP and NEE (r = 0.78 and 0.75, respectively) when using the MODIS and MERRA inputs in the TCF model, compared to R_{eco} and CH_4 ($r = 0.84$ and 0.86, respectively).

Seasonal changes in nutrient availability may have contributed to some of the tower and TCF differences for GPP (Lund et al., 2010); although one peatland study reported that these limitations on plant productivity could be detected indirectly by MODIS NDVI retrievals (Schubert et al., 2010b). It is more likely that the reduced correspondence between the TCF model and tower EC based GPP estimates resulted from a combination of factors including substantial fluctuations and uncertainty in MERRA SW_{rad} (Yi et al., 2011), uncertainty in the satellite NDVI and resulting FPAR records due to residual snow cover and surface water (Delbert et al., 2005), and not accounting for community specific phenology in the LUE algorithm. High latitude studies have reported difficulty in using NDVI to determine the start of spring bud burst and seasonal variability in leaf development (Huemmrich et al., 2010a). Evaluating other portions of the visible spectrum, including blue and green reflectance, in addition to NDVI has helped to alleviate this problem in remote sensing applications (Marushchak et al., 2013) and should be considered in subsequent studies. Incorporating phenological constraints into the TCF LUE model may also be necessary to better characterize early season changes in GPP, especially for plant communities such as *E. vaginatum* that are sensitive to active layer depth (Parmentier et al., 2011a; Natali et al., 2012). Also considering T_s in the TCF LUE model may help to better account for prolonged periods of GPP in the autumn that can occur even after $T_{min} \leq 0\,^{\circ}C$ if water is still available within the root zone (Christiansen et al., 2012). A study by Yi et al. (2013) attempted to address this problem by incorporating satellite passive microwave-based freeze/thaw records (37 GHz) to constrain GPP according to frozen, transitional, or non-frozen surface moisture states but did not report a significant improvement, likely due to the coarse (25 km resolution) freeze/thaw retrievals.

The results from our satellite and reanalysis based TCF model assessment of annual NECB for the six northern EC tower sites indicate that CH_4 emissions reduced the terrestrial net carbon sink by 23 % relative to NEE. Although GPP at the Lena River and Barrow sites mitigated GWP additions from R_{eco} and CH_4 in two of the years examined, in most years the tower sites were GWP contributors by approximately $165 \pm 128\,g\,CO_2eq\,m^{-2}\,yr^{-1}$ when considering the impact of CH_4 on atmospheric forcing over a 100 yr time span. These results are in agreement with other model-based analyses for the Arctic (McGuire et al., 2010) and emphasize the importance of evaluating CO_2 and CH_4 emissions simultaneously when quantifying the terrestrial carbon balance and GWP for northern peatland and tundra ecosystems (Christensen et al., 2012; Olefeldt et al., 2012). However, on-going efforts are needed to better inform landscape scale spatial/temporal variability in soil moisture, temperature and vegetation controls on CO_2 and CH_4 fluxes for future model assessments using a combined network of in-situ soil measurements and strategically placed EC tower sites (Sturtevant and Oechel, 2013), and regional airborne surveys of EC flux. The upcoming SMAP mission may also help to determine landscape sub-surface soil moisture and thermal constraints on northern carbon fluxes through relatively fine scale (3 km resolution) and lower frequency ($\leq$ 1.4 GHz) microwave retrievals with enhanced soil penetration (Entekhabi et al., 2010; Kimball et al., 2012), complimented by recent improvements in Arctic-specific reanalysis data (Bromwich et al., 2010). These advances, in conjunction with a suitable model framework to quantify ecosystem NEE and the relative influence of CH_4 emissions on the NECB, provide the necessary steps forward to better constrain regional carbon emission estimates and to assess changes in the northern carbon sink.

Supplementary material related to this article is available online at http://www.biogeosciences-discuss.net/10/16491/2013/bgd-10-16491-2013-supplement.pdf.

Acknowledgements. Financial support for this study was provided by the NASA Terrestrial Ecology and Science Terra and Aqua programs (NNX09AP52G, NNX11AD46G) and the NESSF program (NNX13AM92H) with work performed at The University of Montana under contract to the National Aeronautics and Space Administration. Additional support was also provided by the National Science Foundation ARC (1204263) and through the Helmholtz Association (Helmholtz Young Investigators Group, grant VH-NG-821).

References

Alstad, K. P. and Whiticar, M. J.: Carbon and hydrogen isotope ratio characterization of methane dynamics for Fluxnet Peatland Ecosystems, Org. Geochem., 42, 548–558, 2011.

Aurela, M., Laurila, T., and Tuovinen, J.: Annual CO_2 balance of a subarctic fen in northern Europe: importance of wintertime efflux, J. Geophys. Res., 107, ACH 17-1–17-12, doi:10.1029/2002JD002055, 2002.

Aurela, M., Riutta, T., Laurila, T. Tuovinen, J.-P., Vesala, T., Tuittila, E.-S., Rinne, J., Haapanala, S., and Laine, J.: CO_2 exchange of a sedge fen in southern Finland-the impact of a drought period, Tellus B, 59, 826–837, 2007.

Badawy, B., Rödenbeck, C., Reichstein, M., Carvalhais, N., and Heimann, M.: Technical Note: The Simple Diagnostic Photosynthesis and Respiration Model (SDPRM), Biogeosciences, 10, 6485–6508, doi:10.5194/bg-10-6485-2013, 2013.

Baldocchi, D.: "Breathing" of the terrestrial biosphere: lessons learned from a global network of carbon dioxide flux measurement systems, Aust. J. Bot., 56, 1–26, 2008.

Beck, P. S. A. and Goetz, S. J.: Satellite observations of high northern latitude vegetation productivity changes between 1982–2008: ecological variability and regional differences, Environ. Res. Lett., 6, 045501, doi:10.1088/1748-9326/6/4/045501, 2011.

BGD
10, 16491–16549, 2013

A satellite data driven biophysical modeling

J. D. Watts et al.

Boike, J., Wille, C., and Abnizova, A.: Climatology and summer energy and water balance of polygonal tundra in the Lena River Delta, Siberia, J. Geophys. Res., 113, G03025, doi:10.1029/2007JG000540, 2008.

Boucher, O., Friedlingstein, P., Collins, B., and Shine, K. P.: The indirect global warming potential and global temperature change potential due to methane oxidation, Environ. Res. Lett., 4, 044007, doi:10.1088/1748-9326/4/4/044007, 2009.

Bromwich, D., Kuo, Y.-H., Serreze, M., Walsh, J., Bai, L. S., Barlage, M., Hines, K., and Slater, A.: Arctic system reanalysis: call for community involvement, EOS T. Am. Geophys. Un., 91, 13–14, 2010.

Chanton, J. P.: The effect of gas transport on the isotope signature of methane in wetlands, Org. Geochem., 36, 753–768, 2005.

Choudhury, B. J.: Carbon use efficiency, and net primary productivity of terrestrial vegetation, Adv. Space Res., 26, 1105–1108, 2000.

Christensen, T. R., Jackowicz-Korczyński, M., Aurela, M., Crill, P., Heliasz, M., Mastepanov, M., and Friborg, T.: Monitoring the multi-year carbon balance of a subarctic palsa mire with micrometeorological techniques, AMBIO, 41, 207–217, 2012.

Christiansen, C. T., Schmidt, N. M., and Michelsen, A.: High Arctic dry heath CO_2 exchange during the early cold season, Ecosystems, 3224–3236, doi:10.1007/s10021-012-9569-4, 2012.

Clark, D. B., Mercado, L. M., Sitch, S., Jones, C. D., Gedney, N., Best, M. J., Pryor, M., Rooney, G. G., Essery, R. L. H., Blyth, E., Boucher, O., Harding, R. J., Huntingford, C., and Cox, P. M.: The Joint UK Land Environment Simulator (JULES), model description – Part 2: Carbon fluxes and vegetation dynamics, Geosci. Model Dev., 4, 701–722, doi:10.5194/gmd-4-701-2011, 2011.

Connolly, J., Roulet, N. T., Seaquist, J. W., Holden, N. M., Lafleur, P. M., Humphreys, E. R., Heumann, B. W., and Ward, S. M.: Using MODIS derived *f*PAR with ground based flux tower measurements to derive the light use efficiency for two Canadian peatlands, Biogeosciences, 6, 225–234, doi:10.5194/bg-6-225-2009, 2009.

Corbett, J. E., Tfaily, M. M., Burdige, D. J., Cooper, W. T., Glaser, P. H., and Chanton, J. P.: Partitioning pathways of CO_2 production in peatlands with stable carbon isotopes, Biogeochemistry, 327–340, doi:10.1007/s10533-012-9813-1, 2012.

Davidson, E. A. and Janssens, I. A.: Temperature sensitivity of soil carbon decomposition and feedbacks to climate change, Nature, 440, 165–173, 2006.

Delbart, N., Kergoat, L., Le Toan, T., Lhermitte, J., and Ghislain, P.: Determination of phenological dates in boreal regions using normalized difference water index, Remote Sens. Environ., 97, 26–38, doi:10.1016/j.rse.2005.03.011, 2005.

Dijkstra, F. A., Prior, S. A., Runion, G. B., Torbert, H. A., Tian, H., Lu, C., and Venterea, R. T.: Effects of elevated carbon dioxide and increased temperature on methane and nitrous oxide fluxes: evidence from field experiments, Front. Ecol. Environ., 10, 520–527, 2012.

Dlugokencky, E. J., Bruhwiler, L., White, J. W. C., Emmons, L. K., Novelli, P. C., Montzka, S. A., Masarie, K. A., Lang, P. M., Crotwell, A. M., Miller, J. B., and Gatti, L. V.: Observational constraints on recent increases in the atmospheric CH_4 burden, Geophys. Res. Lett., 36, L18803, doi:10.1029/2009GL039780, 2009.

Dolman, A. J., van der Werf, G. R., van der Molen, M. K., Ganssen, G., Erisman, J.-W., and Strengers, B.: A carbon cycle science uptake since IPCC AR-4, AMBIO, 39, 402–412, 2010.

Dorrepaal, E., Toet, S., van Logtestijn, R. S. P., Swart, E., van de Weg, M. J., Callaghan, T. V., and Aerts, R.: Carbon respiration from subsurface peat accelerated by climate warming in the subarctic, Nature, 460, 616–619, 2009.

Elberling, B., Tamstorf, M. P., Michelsen, A., Arndal, M. F., Sigsgaard, C., Illeris, L., Bay, C., Hansen, B. U., Christensen, T. R., Hansen, E. S., Jakobsen, B. H., and Beyens, L.: Soil and plant community-characteristics and dynamics at Zackenberg, Adv. Ecol. Res., 40, 223–248, 2008.

Elberling, B., Askaer, L., Jørgensen, C. J., Joensen, H. P., Kühl, M., Glud, R. N., and Lauritsen, F. R.: Linking soil O_2, CO_2, and CH_4 concentrations in a wetland soil: implications for CO_2 and CH_4 fluxes, Environ. Sci. Technol., 45, 3393–3399, 2011.

Elmendorf, S. C., Henry, G. H. R., Hollister, R. D., Björk, R. G., Bjorkman, A. D., Callaghan, T. V., Collier, L. S., Cooper, E. J., Cornelissen, J. H. C., Day, T. A., Fosaa, A. M., Gould, W. A., Grétarsdóttir, J., Harte, J., Hermanutz, L., Hik, D. S., Hofgaard, A., Jarrad, F., Jónsdóttir, I. S., Keuper, F., Klanderud, K., Klein, J. A., Koh, S., Kudo, G., Lang, S. I., Loewen, V., May, J. L., Mercado, J., Michelsen, A., Molau, U., Myers-Smith, I. H., Oberbauer, S. F., Pieper, S., Post, E., Rixen, C., Robinson, C. H., Schmidt, N. M., Shaver, G. R., Stenström, A., Tolvanen, A., Totland, Ø., Troxler, T., Wahren, C.-H., Webber, P. J., Welker, J. M., and Wookey, P. A.: Global assessment of experimental climate warming on tundra vegetation: heterogeneity over space and time, Ecol. Lett., 15, 164–175, 2012.

Entekhabi, D., Njoku, E. G., O'Neill, P. E., Kellogg, K. H., Crow, W. T., Edelstein, W. N., Entin, J. K., Goodman, S. D., Jackson, T. J., Johnson, J., Kimball, J. S., Piepmeier, J. R.,

BGD
10, 16491–16549, 2013

Koster, R. D., Martin, N., McDonald, K. C., Moghaddam, M., Moran, S., Reichle, R., Shi, J.-C., Spencer, M. W., Thurman, S. W., Tsang, L., and Van Zyl, J.: The Soil Moisture Active Passive (SMAP) mission, Proc. IEEE, 98, 704–716, 2010.
Forbrich, I., Kutzbach, L., Wille, C., Becker, T., Wu, J., and Wilmking, M.: Cross-evaluation of measurements of peatland methane emissions on microform and ecosystem scales using high-resolution landcover classification and source weight modeling, Agr. Forest Meterol., 151, 864–874, 2011.
Frenzel, P. and Rudolph, J.: Methane emission from a wetland plant: the role of CH_4 oxidation in *Eriophorum*, Plant Soil, 202, 27–32, 1998.
Gedney, N. and Cox, P. M.: The sensitivity of global climate model simulations to the representation of soil moisture heterogeneity, J. Hydrometeorol., 4, 1265–1275, 2003.
Glanville, H. C., Hill, P. W., Maccarone, L. D., Golyshin, P. N., Murphy, D. V., and Jones, D. L.: Temperature and soil water controls on vegetation emergence, microbial dynamics, and soil carbon and nitrogen fluxes in a high Arctic tundra ecosystem, Funct. Ecol., 26, 1366–1380, 2012.
Grosse, W., Armstrong, J., and Armstrong, W.: A history of pressurized gas-flow studies in plants, Aquat. Biol., 54, 57–100, 1996.
Hargreaves, K. J., Fowler, D., Pitcairn, C. E. R., and Aurela, M.: Annual methane emission from Finnish mires estimated from eddy covariance campaign measurements, Theor. Appl. Climatol., 70, 203–213, 2001.
Hicks Pries, C. E., Schuur, E. A. G., and Crummer, K. G.: Thawing permafrost increases old soil and autotrophic respiration in tundra: partitioning ecosystem respiration using $\delta^{13}C$ and $\delta^{14}C$, Glob. Change Biol., 19, 649–661, 2013a.
Hicks Pries, C. E., Schuur, E. A. G., Vogel, J. G., and Natali, S. M.: Moisture drives surface decomposition in thawing tundra, J. Geophys. Res.-Biogeo., 118, 1–11, 2013b.
Högström, U.: Non-dimensional wind and temperature profiles in the atmospheric surface layer: a re-evaluation, Bound.-Lay. Meteorol., 42, 55–78, 1988.
Hudson, J. M. G., Henry, G. H. R., and Cornwell, W. K.: Taller and larger: shifts in Arctic tundra leaf traits after 16 years of experimental warming, Glob. Change Biol., 17, 1013–1021, 2011.
Huemmrich, K. F., Gamon, J. A., Tweedie, C. E., Oberbauer, S. F., Kinoshita, G., Houston, S., Kuchy, A., Hollister, R. D., Kwon, H., Mano, M., Harazono, Y., Webber, P. J., and Oechel, W. C.: Remote sensing of tundra gross ecosystem productivity and light use ef-

ficiency under varying temperature and moisture conditions, Remote Sens. Environ., 114, 481–489, 2010a.

Huemmrich, K. F., Kinoshita, G., Gamon, A., Houston, S., Kwon, H., and Oechel, W. C.: Tundra carbon balance under varying temperature and moisture regimes, J. Geophys. Res., 115, G00102, doi:10.1029/2009JG001237, 2010b.

Hugelius, G., Routh, J., Kuhry, P., and Crill, P.: Mapping the degree of decomposition and thaw remobilization potential of soil organic matter in discontinuous permafrost terrain, J. Geophys. Res.-Biogeo., G00102, doi:10.1029/2011JG001873, 2012.

Hugelius, G., Tarnocai, C., Broll, G., Canadell, J. G., Kuhry, P., and Swanson, D. K.: The Northern Circumpolar Soil Carbon Database: spatially distributed datasets of soil coverage and soil carbon storage in the northern permafrost regions, Earth Syst. Sci. Data, 5, 3–13, doi:10.5194/essd-5-3-2013, 2013.

Inglett, K. S., Inglett, P. W., Reddy, K. R., and Osborne, T. Z.: Temperature sensitivity of greenhouse gas production in wetland soils of different vegetation, Biogeochemistry, 108, 77–90, 2012.

Ise, T. and Moorcroft, P. R.: The global-scale temperature and moisture dependencies of soil organic carbon decomposition: an analysis using a mechanistic decomposition model, Biogeochemistry, 80, 217–231, 2006.

Ise, T., Dunn, A. L., Wofsy, S. C., and Moorcroft, P. R.: High sensitivity of peat decomposition to climate change through water-table feedback, Nat. Geosci., 1, 763–766, 2008.

Jackowicz-Korczyński, M., Christensen, T. R., Bäckstrand, K., Crill, P., Friborg, T., Mastepanov, M., and Ström, L.: Annual cycle of methane emission from a subarctic peatland, J. Geophys. Res.-Biogeo., 115, G02009, doi:10.1029/2008JG000913, 2010.

Joabsson, A., Christensen, T. R., and Wallén, B.: Vascular plant controls on methane emissions from northern peatforming wetlands, TREE, 14, 385–388, 1999.

Kane, E. S.: Ecosystem carbon storage: squeezing the Arctic carbon balloon, Nature Clim. Change, 2, 841–842, 2012.

Kettridge, N., Binley, A., Green, S. M., and Baird, A. J.: Ebullition events monitored from northern peatlands using electrical imaging, J. Geophys. Res., 116, G04004, doi:10.1029/2010JG001561, 2011.

Kim, Y., Kimball, J. S., Zhang, K., and McDonald, K. C.: Satellite detection of increasing Northern Hemisphere non-frozen seasons from 1979 to 2008: implications for regional vegetation growth, Remote Sens. Environ., 121, 472–487, 2012.

BGD
10, 16491–16549, 2013
A satellite data driven biophysical modeling
J. D. Watts et al.

Kimball, J. S., Jones, L. A., Zhang, K., Heinsch, F. A., McDonald, K. C., and Oechel, W. C.: A satellite approach to estimate land-atmosphere CO_2 exchange for boreal and Arctic biomes using MODIS and AMSR-E, IEEE T. Geosci. Remote, 47, 569–587, 2009.

Kimball, J. S., Reichle, R., McDonald, K., and Njoku, E.: Soil Moisture Active Passive (SMAP) Algorithm Theoretical Basis Document (ATBD): SMAP Level 4 Carbon Data Product (L4_C), Initial Release v. 1, Jet Propulsion Laboratory, California Institute of Technology,, 73 pp., 2012.

King, D. A., Turner, D. P., and Ritts, W. D.: Parameterization of a diagnostic carbon cycle model for continental scale application, Remote Sens. Environ., 115, 1653–1664, 2011.

Kip, N., van Winden, J. F., Pan, Y., Bodrossy, L., Reichart, G.-J., Smolders, A. J. P., Jetten, M. S. M., Damsté, J. S. S., and Op den Camp, H. J. M.: Global prevalence of methane oxidation by symbiotic bacteria in peat-moss ecosystems, Nat. Geosci., 3, 617–621, 2010.

Kutzbach, L., Wille, C., and Pfeiffer, E.-M.: The exchange of carbon dioxide between wet arctic tundra and the atmosphere at the Lena River Delta, Northern Siberia, Biogeosciences, 4, 869–890, doi:10.5194/bg-4-869-2007, 2007.

Le Mer, J. and Roger, P.: Production, oxidation, emission and consumption of methane by soils: a review, Eur. J. Soil Biol., 37, 25–50, 2001.

Levy, P. E., Burden, A., Cooper, M. D., Dinsmore, K. J., Drewer, J., Evans, C., Fowler, D., Gaiawyn, J., Gray, A., Jones, S. K., Jones, T., McNamara, N. P., Mills, R., Ostle, N., Sheppard, L. J., Skiba, U., Sowerby, A., Ward, S. E., and Zieliński, P.: Methane emissions from soils: synthesis and analysis of a large UK data set, Glob. Change Biol., 18, 1657–1669, 2012.

Lund, M., Lafleur, P. M., Roulet, N. T., Lindroth, A., Christensen, T. R., Aurela, M., Chojnicki, B. H., Flanagan, L. B., Humphreys, E. R., Laurila, T., Oechel, W. C., Olejnik, J., Rinne, J., Schubert, P., and Nilsson, M. B.: Variability in exchange of CO_2 across 12 northern peatland and tundra sites, Glob. Change Biol., 16, 2436–2448, 2010.

Lloyd, J. and Taylor, J. A.: On the temperature dependence of soil respiration, Funct. Ecol., 8, 315–323, 1994.

Marushchak, M. E., Kiepe, I., Biasi, C., Elsakov, V., Friborg, T., Johansson, T., Soegaard, H., Virtanen, T., and Martikainen, P. J.: Carbon dioxide balance of subarctic tundra from plot to regional scales, Biogeosciences, 10, 437–452, doi:10.5194/bg-10-437-2013, 2013.

McCallum, I., Franklin, O., Moltchanova, E., Merbold, L., Schmullius, C., Shvidenko, A., Schepaschenko, D., and Fritz, S.: Improved light and temperature responses for light use efficiency based GPP models, Biogeosciences Discuss., 10, 8919–8947, doi:10.5194/bgd-10-8919-2013, 2013.

McGuire, A. D., Hayes, D. J., Kicklighter, D. W., Manizza, M., Zhuang, Q., Chen, M., Follows, M. J., Gurney, K. R., McClelland, J. W., and Melillo, J. M.: An analysis of the carbon balance of the Arctic Basin from 1997 to 2006, Tellus B, 62, 455–474, 2010.

McGuire, A. D., Christensen, T. R., Hayes, D., Heroult, A., Euskirchen, E., Kimball, J. S., Koven, C., Lafleur, P., Miller, P. A., Oechel, W., Peylin, P., Williams, M., and Yi, Y.: An assessment of the carbon balance of Arctic tundra: comparisons among observations, process models, and atmospheric inversions, Biogeosciences, 9, 3185–3204, doi:10.5194/bg-9-3185-2012, 2012.

Meng, L., Hess, P. G. M., Mahowald, N. M., Yavitt, J. B., Riley, W. J., Subin, Z. M., Lawrence, D. M., Swenson, S. C., Jauhiainen, J., and Fuka, D. R.: Sensitivity of wetland methane emissions to model assumptions: application and model testing against site observations, Biogeosciences, 9, 2793–2819, doi:10.5194/bg-9-2793-2012, 2012.

Merbold, L., Kutsch, W. L., Corradi, C., Kolle, O., Rebmann, C., Stoy, P. C., Zimov, S. A., and Schulze, E.-D.: Artificial drainage and associated carbon fluxes (CO_2/CH_4) in a tundra ecosystem, Glob. Change Biol., 15, 2599–2614, 2009.

Moosavi, S. C. and Crill, P. M.: Controls on CH_4 and CO_2 emissions along two moisture gradients in the Canadian boreal zone, J. Geophys. Res.-Atmos., 102, 261–277, 1997.

Natali, S. M., Schuur, E. A., and Rubin, R. L.: Increased plant productivity in Alaskan tundra as a result of experimental warming of soil and permafrost, J. Ecol., 488–498, 2012.

Oberbauer, S. F., Cheng, W., Gillespie, C. T., Ostendorf, B., Sala, A., Gebauer, G., Virginia, R. A., and Tenhunen, J. D.: Landscape patterns of carbon dioxide exchange in tundra ecosystems, in: Ecological Studies, Vol. 120, edited by: Reynolds, J. F. and Tenhunen, J. D., Springer-Verlag, Berlin, Heidelberg, 223–256, 1996.

Olefeldt, D., Roulet, N. T., Bergeron, O., Crill, P., Bäckstrand, K., and Christensen, T. R.: Net carbon accumulation of a high-latitude permafrost palsa mire similar to permafrost-free peatlands, Geophys. Res. Lett., 39, 589–603, doi:10.1029/2011GL050355, 2012.

Olefeldt, D., Turetsky, M. R., Crill, P. M., and McGuire, A. D.: Environmental and physical controls on northern terrestrial methane emissions across permafrost zones, Glob. Change Biol., 19, 589–603, 2013.

Olivas, P. C., Oberbauer, S. F., Tweedie, C. E., Oechel, W. C., and Kuchy, A.: Responses of CO_2 flux components of Alaskan Coastal Plain tundra to shifts in water table, J. Geophys. Res.-Biogeo., 115, G00105, doi:10.1029/2009JG001254, 2010.
Olsrud, M. and Christensen, T. R.: Carbon partitioning in a wet and a semiwet subarctic mire ecosystem based on in situ ^{14}C pulse labeling, Soil Biol. Biochem., 43, 231–239, 2011.
Parmentier, F. J. W., van der Molen, M. K., van Huissteden, J., Karsanaev, S. A., Kononov, A. V., Suzdalov, D. A., Maximov, T. C., and Dolman, A. J.: Longer growing seasons do not increase net carbon uptake in the northeastern Siberian tundra, J. Geophys. Res.-Biogeo., 116, G4, doi:10.1029/2011JG001653, 2011a.
Parmentier, F. J. W., van Huissteden, J., van der Molen, M. K., Schaepman-Strub, G., Karsanaev, S. A., Maximov, T. C., and Dolman, A. J.: Spatial and temporal dynamics in eddy covariance observations of methane fluxes at a tundra site in northeastern Siberia, J. Geophys. Res.-Biogeo., 116, G03016, doi:10.1029/2010JG001637, 2011b.
Parmentier, F. J. W., van Huissteden, J., Kip, N., Op den Camp, H. J. M., Jetten, M. S. M., Maximov, T. C., and Dolman, A. J.: The role of endophytic methane-oxidizing bacteria in submerged *Sphagnum* in determining methane emissions of Northeastern Siberian tundra, Biogeosciences, 8, 1267–1278, doi:10.5194/bg-8-1267-2011, 2011c.
Parmentier, F. J. W., Christensen, T. R., Sorensen, L. L., Rysgaard, S., McGuire, A. D., Miller, P. A., and Walker, D. A.: The impact of lower sea-ice extent on Arctic greenhouse-gas exchange, Nature Clim. Change, 3, 195–202, 2013.
Peng, D., Zhang, B., and Liu, L.: Comparing spatiotemporal patterns in Eurasian FPAR derived from two NDVI-based methods, Int. J. Digital Earth, 5, 283–298, 2012.
Petrescu, A. M. R., van Beek, L. P. H., van Huissteden, J., Prigent, C., Sachs, T., Corradi, C. A. R., Parmentier, F. J. W., and Dolman, A. J.: Modeling regional to global CH_4 emissions of boreal and arctic wetlands, Global Biogeochem. Cy., 24, GB4009, doi:10.1029/2009GB003610, 2010.
Porter, C. H., Jones, J. W., Adiku, S., Gijsman, A. J., Gargiulo, O., and Naab, J. B.: Modeling organic carbon and carbon-mediated soil processes in DSSAT V4.5, Oper. Res. Int. J., 10, 274–278, 2010.
Potter, C., Klooster, S., Hiatt, S., Fladeland, M., Genovese, V., and Gross, P.: Methane emissions from natural wetlands in the United States: Satellite-derived estimation based on ecosystem carbon cycling, Earth Interact., 10, 1–12, 2006.

BGD
10, 16491–16549, 2013

A satellite data driven biophysical modeling

J. D. Watts et al.

Preuss, I., Knoblauch, C., Gebert, J., and Pfeiffer, E.-M.: Improved quantification of microbial CH_4 oxidation efficiency in arctic wetland soils using carbon isotope fractionation, Biogeosciences, 10, 2539–2552, doi:10.5194/bg-10-2539-2013, 2013.
Raupach, M. R.: Influences of local feedbacks on land-air exchanges of energy and carbon, Glob. Change Biol., 4, 477–494, 1998.
Reiche, M., Gleixner, G., and Küsel, K.: Effect of peat quality on microbial greenhouse gas formation in an acidic fen, Biogeosciences, 7, 187–198, doi:10.5194/bg-7-187-2010, 2010.
Reichle, R. H., Koster, R. D., De Lannoy, G. J. M., Forman, B. A., Liu, Q., Mahanama, S. P. P., and Toure, A.: Assessment and enhancement of MERRA land surface hydrology estimates, J. Climate, 24, 6322–6338, 2011.
Rienecker, M. M., Suarez, M. J., Gelaro, R., Todling, R., Bacmeister, J., Liu, E., Bosilovich, M. G., Schubert, S. D., Takacs, L., Kim, G.-K., Bloom, S., Chen, J., Collins, D., Conaty, A., da Silva, A., Gu, W., Joiner, J., Koster, R. D., Lucchesi, R., Molod, A., Owens, T., Pawson, S., Pegion, P., Redder, C. R., Reichle, R., Robertson, F. R., Ruddick, A. G., Sienkiewicz, M., and Woollen, J.: MERRA: NASA's Modern-Era Retrospective Analysis for Research and Applications, J. Climate, 24, 3624–3648, 2011.
Riley, W. J., Subin, Z. M., Lawrence, D. M., Swenson, S. C., Torn, M. S., Meng, L., Mahowald, N. M., and Hess, P.: Barriers to predicting changes in global terrestrial methane fluxes: analyses using CLM4Me, a methane biogeochemistry model integrated in CESM, Biogeosciences, 8, 1925–1953, doi:10.5194/bg-8-1925-2011, 2011.
Rinne, J., Riutta, T., Pihlatie, M., Aurela, M., Haapanala, S., Tuovinen, J., Tuittila, E., and Vesala, T.: Annual cycle of methane emission from a boreal fen measured by the eddy covariance technique, Tellus B, 59, 449–457, 2007.
Riutta, T., Laine, J., Aurela, M., Rinne, J., Vesala, T., Laurila, T., Haapanala, S., Pihlatie, M., and Tuittila, E.-S.: Spatial variation in plant community functions regulates carbon gas dynamics in a boreal fen ecosystems, Tellus B, 59, 838–852, 2007.
Roberts, J.: The influence of physical and physiological characteristics of vegetation on their hydrological response, Hydrol. Process., 14, 2885–2901, 2000.
Rosenberry, D. O., Glaser, P. H., and Siegel, D. I.: The hydrology of northern peatlands as affected by biogenic gas: current developments and research needs, Hydrol. Process., 20, 3601–3610, 2006.

Running, S. W., Nemani, R. R., Heinsch, F. A., Zhao, M., Reeves, M., and Hashimoto, H.: A continuous satellite-derived measure of global terrestrial primary production, BioScience, 54, 547–560, 2004.

Sachs, T., Wille, C., Boike, J., and Kutzbach, L.: Environmental controls on ecosystem-scale CH_4 emission from polygonal tundra in the Lena River Delta, Siberia, J. Geophys. Res., 113, 3096–3110, doi:10.1029/2007JG000505, 2008.

Sachs, T., Giebels, M., Boike, J., and Kutzbach, L.: Environmental controls on CH_4 emission from polygonal tundra on the microsite scale in the Lena river delta, Siberia, Glob. Change Biol., 16, 3096–3110, 2010.

Schneider von Deimling, T., Meinshausen, M., Levermann, A., Huber, V., Frieler, K., Lawrence, D. M., and Brovkin, V.: Estimating the near-surface permafrost-carbon feedback on global warming, Biogeosciences, 9, 649–665, doi:10.5194/bg-9-649-2012, 2012.

Schubert, P., Eklundh, L., Lund, M., and Nilsson, M.: Estimating northern peatland CO_2 exchange from MODIS time series data, Remote Sens. Environ, 114, 1178–1189, 2010a.

Schubert, P., Lund, M., Ström, L., and Eklundh, L.: Impact of nutrients on peatland GPP estimations using MODIS time series, Remote Sens. Environ., 114, 2137–2145, 2010b.

Schubert, P., Lagergren, F., Aurela, M., Christensen, T., Grelle, A., Heliasz, M., Klemedtsson, L., Lindroth, A., Pilegaard, K., Vesala, T., and Eklundh, L.: Modeling GPP in the Nordic forest landscape with MODIS time series data-Comparison with the MODIS GPP product, Remote Sens. Environ., 126, 136–147, 2012.

Schuur, E. A. G., Vogel, J. G., Crummer, K. G., Lee, H., Sickman, J. O., and Osterkamp, T. E.: The effect of permafrost thaw on old carbon release and net carbon exchange from tundra, Nature, 459, 556–559, 2009.

Shiklomanov, N. I., Streletskiy, D. A., Nelson, F. E., Hollister, R. D., Romanovsky, V. E., Tweedie, C. E., Bockheim, J. G., and Brown, J.: Decadal variations of active-layer thickness in moisture-controlled landscapes, Barrow, Alaska, J. Geophys. Res., 115, G00104, doi:10.1029/2009JG001248, 2010.

Sigsgaard, C.: Guidelines and sampling procedures for the geographical monitoring programme of Zackenberg Basic, Zackenberg Ecological Research Operations, GeoBasis, 124 pp., 2011.

Sitch, S., McGuire, A. D., Kimball, J., Gedney, N., Gamon, J., Engstrom, R., Wolf, A., Zhuang, Q., Clein, J., and McDonald, K. C.: Assessing the carbon balance of circumpolar Arctic tundra using remote sensing and process modeling, Ecol. App., 17, 213–234, 2007.

BGD
10, 16491–16549, 2013

Sjögersten, S. and Wookey, P. A.: The impact of climate change on ecosystem carbon dynamics at the Scandinavian mountain birch forest-tundra heath ecotone, AMBIO, 38, 2–10, 2009.
Solano, R., Didan, D., Jacobson, A., and Huete, A.: MODIS Vegetation Index User's Guide (MOD13 Series), Version 2.0, Vegetation Index and Phenology Lab, The University of Arizona, 42 pp., 2010.
Spahni, R., Wania, R., Neef, L., van Weele, M., Pison, I., Bousquet, P., Frankenberg, C., Foster, P. N., Joos, F., Prentice, I. C., and van Velthoven, P.: Constraining global methane emissions and uptake by ecosystems, Biogeosciences, 8, 1643–1665, doi:10.5194/bg-8-1643-2011, 2011.
Street, L. E., Stoy, P. C., Sommerkorn, M., Fletcher, B. J., Sloan, V. L., Hill, T. C., and Williams, M.: Seasonal bryophyte productivity in the sub-Arctic: a comparison with vascular plants, Funct. Ecol., 26, 365–378, 2012.
Ström, L., Ekberg, A., Mastepanov, M., and Christensen, T. R.: The effect of vascular plants on carbon turnover and methane emissions from a tundra wetland, Glob. Change Biol., 9, 1185–1192, 2003.
Ström, L., Mastepanov, M., and Christensen, T. R.: Species-specific effects of vascular plants on carbon turnover and methane emissions from wetlands, Biogeochemistry, 75, 65–82, 2005.
Sturtevant, C. S. and Oechel, W. C.: Spatial variation in landscape-level CO_2 and CH_4 fluxes from arctic coastal tundra: influence from vegetation, wetness, and the thaw lake cycle, Glob. Change Biol., 19, 2853–2866, doi:10.1111/gbc.12247, 2013.
Sturtevant, C. S., Oechel, W. C., Zona, D., Kim, Y., and Emerson, C. E.: Soil moisture control over autumn season methane flux, Arctic Coastal Plain of Alaska, Biogeosciences, 9, 1423–1440, doi:10.5194/bg-9-1423-2012, 2012.
Sun, X., Song, C., Guo, Y., Wang, X., Yang, G., Li, Y., Mao, R., and Lu, Y.: Effect of plants on methane emissions from a temperate marsh in different seasons, Atmos. Environ., 60, 277–282, 2012.
Tagesson, T., Mastepanov, M., Tamstorf, M. P., Eklundh, L., Schubert, P., Ekberg, A., Sigsgaard, C., Christensen, T. R., and Ström, L.: High-resolution satellite data reveal an increase in peak growing season gross primary production in a high-Arctic wet tundra ecosystem 1992–2008, Int. J. Appl. Earth Obs., 18, 407–416, 2012a.
Tagesson, T., Mölder, M., Mastepanov, M., Sigsgaard, C., Tamstorf, M. P., Lund, M., Falk, J. M., Lindroth, A., Christensen, T. R., and Ström, L.: Land-atmosphere exchange of methane from

soil thawing to soil freezing in a high-Arctic wet tundra ecosystem, Glob. Change Biol., 18, 1928–1940, 2012b.
Tagesson, T., Mastepanov, M., Mölder, M., Tamstorf, M. P., Eklundh, L., Smith, B., Sigsgaard, C., Lund, M., Ekberg, A., Falk, J. M., Friborg, T., Christensen, T. R., and Ström, L.: Modelling of growing season methane fluxes in a high-Arctic wet tundra ecosystem 1997–2010 using in situ and high-resolution satellite data, Tellus B, 65, 19722, doi:10.3402/tellusb.v65i0.19722, 2013.
Tian, H., Xu, X., Liu, M., Ren, W., Zhang, C., Chen, G., and Lu, C.: Spatial and temporal patterns of CH_4 and N_2O fluxes in terrestrial ecosystems of North America during 1979–2008: application of a global biogeochemistry model, Biogeosciences, 7, 2673–2694, doi:10.5194/bg-7-2673-2010, 2010.
Turetsky, M. R., Treat, C. C., Waldrop, M. P., Waddington, J. M., Harden, J. W., and McGuire, D.: Short-term response of methane fluxes and methanogen activity to water table and soil warming manipulations in an Alaskan peatland, J. Geophys. Res., 113, G00A10, doi:10.1029/2007JG000496, 2008.
van Huissteden, J., van den Bos, R., and Marticorena Alvarez, I.: Modelling the effect of water-table management on CO_2 and CH_4 fluxes from peat soils, Neth. J. Geosci., 85, 3–18, 2006.
van Hulzen, J. B., Segers, R., van Bodegom, P. M., and Leffelaar, P. A.: Temperature effects on soil methane production: an explanation for observed variability, Soil Biol. Biochem., 31, 1919–1929, 1999.
Verry, E. S., Boelter, D. H., Paivanen, J., Nichols, D. S., Malterer, T., and Gafni, A., in: Peatland Biogeochemistry and Watershed Hydrology at the Marcell Experimental Forest, edited by: Kolka, R., Sebestyen, S., Verry, E. S., and Brooks, K., CRC Press, Boca Raton, 135–176, 2011.
von Fischer, J. C. and Hedin, L. O.: Controls on soil methane fluxes: tests of biophysical mechanisms using stable isotope tracers, Global Biogeochem. Cy., 21, GB2007, doi:10.1029/2006GB002687, 2007.
von Fischer, J. C., Rhew, R. C., Ames, G. M., Fosdick, B. K., and von Fischer, P. E.: Vegetation height and other controls of spatial variability in methane emissions from the Arctic coastal tundra at Barrow, Alaska, J. Geophys. Res., 115, G00103, doi:10.1029/2009JG001283, 2010.

Wagner, D., Kobabe, S., and Liebner, S.: Bacterial community structure and carbon turnover in permafrost-affected soils of the Lena Delta, northeastern Siberia, Can. J. Microbiol., 55, 73–83, 2009.

Walter, B. P. and Heimann, M.: A process-based, climate-sensitive model to derive methane emissions from natural wetlands: application to five wetland sites, sensitivity to model parameters, and climate, Global Biogeochem. Cy., 14, 745–765, 2000.

Wania, R., Ross, I., and Prentice, I. C.: Implementation and evaluation of a new methane model within a dynamic global vegetation model: LPJ-WHyMe v1.3.1, Geosci. Model Dev., 3, 565–584, doi:10.5194/gmd-3-565-2010, 2010.

Wania, R., Melton, J. R., Hodson, E. L., Poulter, B., Ringeval, B., Spahni, R., Bohn, T., Avis, C. A., Chen, G., Eliseev, A. V., Hopcroft, P. O., Riley, W. J., Subin, Z. M., Tian, H., van Bodegom, P. M., Kleinen, T., Yu, Z. C., Singarayer, J. S., Zürcher, S., Lettenmaier, D. P., Beerling, D. J., Denisov, S. N., Prigent, C., Papa, F., and Kaplan, J. O.: Present state of global wetland extent and wetland methane modelling: methodology of a model inter-comparison project (WETCHIMP), Geosci. Model Dev., 6, 617–641, doi:10.5194/gmd-6-617-2013, 2013.

Watts, J. D., Kimball, J. S., Jones, L. A., Schroeder, R., and McDonald, K. C.: Satellite microwave remote sensing of contrasting surface water inundation changes within the Arctic–Boreal region, Remote Sens. Environ., 127, 223–236, 2012.

Wegner, L. H.: Oxygen transport in waterlogged plants, in: Waterlogging Signalling and Tolerance in Plants, edited by: Mancuso, S. and Shabala, S., Springer-Verlag Berlin Heidelberg, 294 pp., 2010.

Wille, C., Kutzbach, L., Sachs, T., Wagner, D., and Pfeiffer, E.-M.: Methane emission from Siberian arctic polygonal tundra: eddy covariance measurements and modeling, Glob. Change Biol., 14, 1395–1408, 2008.

Wu, J., Roulet, N. T., Sagerfors, J., Nilsson, M. B.: Simulation of six years of carbon fluxes for a sedge-dominated oligotrophic minerogenic peatland in Northern Sweden using the McGill wetland model (MWM), J. Geophys. Res.-Biogeo., 118, 795–807, doi:10.1002/jgrg.20045, 2013.

Yan, H., Wang, S. Q., Billesbach, D., Oechel, W., Zhang, J. H., Meyers, T., Martin, T. A., Matamala, R., Baldocchi, D., Bohrer, G., Bragoni, D., and Scott, R.: Global estimation of evapotranspiration using a leaf area index-based surface energy and water balance model, Remote Sens. Environ., 124, 581–595, 2012.

Yang, R. and Friedl, M. A.: Determination of roughness lengths for heat and momentum over boreal forests, Bound.-Lay. Meterol., 107, 581–603, 2002.
Yi, Y., Kimball, J. S., Jones, L. A., Reichle, R. H., and McDonald, K. C.: Evaluation of MERRA land surface estimates in preparation for the soil moisture active passive mission, J. Climate, 24, 3797–3816, 2011.
Yi, Y., Kimball, J. S., Jones, L. A, Reichle, R. H., Nemani, R., and Margolis, H. A.: Recent climate and fire disturbance impacts on boreal and arctic ecosystem productivity estimated using a satellite-based terrestrial carbon flux model, J. Geophys. Res.-Biogeo., 118, 1–17, 2013.
Yuan, W., Luo, Y., Li, X., Liu, S., Yu, S., Zhou, T., Bahn, M., Black, A., Desai, A. R., Cescatti, A., Marcolla, B., Jacobs, C., Chen, J., Aurela, M., Bernhofer, C., Gielen, B., Bohrer, G., Cook, D. R., Dragoni, D., Dunn, A. L., Gianelle, D., Grünwald, T., Ibrom, A., Leclerc, M. Y., Lindroth, A., Liu, H., Marchesini, L. B., Montagnani, L., Pita, G., Rodeghiero, Rodrigues, A., Starr, G., and Stoy, P. C.: Redefinition and global estimation of basal ecosystem respiration rate, Global Biogeochem. Cy., 25, GB4002, doi:10.1029/2011GB004150, 2011.
Zhang, X., He, J., Zhang, J., Polyakov, I., Gerdes, R., Inoue, J., and Wu, P.: Enhanced poleward moisture transport and amplified northern high-latitude wetting trend, Nature Climate Change, 3, 47–51, 2012a.
Zhang, Y., Sachs, T., Li, C., and Boike, J.: Upscaling methane fluxes from closed chambers to eddy covariance based on a permafrost biogeochemistry integrated model, Glob. Change Biol., 18, 1428–1440, 2012b.
Zhao, M., Heinsch, F. A., Nemani, R. M., and Running, S. W.: Improvements of the MODIS terrestrial gross and net primary production global data set, Remote Sens. Environ., 95, 164–176, 2005.
Zhuang, Q., Melillo, J. M., Kicklighter, D. W., Prinn, R. G., McGuire, A. D., Steudler, P. A., Felzer, B. S., and Hu, S.: Methane fluxes between terrestrial ecosystems and the atmosphere at northern high latitudes during the past century: a retrospective analysis with a process-based biogeochemistry model, Global Biogeochem. Cy., 18, GB3010, doi:10.1029/2004GB002239, 2004.
Zona, D., Oechel, W. C., Kochendorfer, J., Paw, U., K. T., Salyuk, A. N., Olivas, P. C., Oberbauer, S. F., and Lipson, D. A.: Methane fluxes during the initiation of a large-scale water table manipulation experiment in the Alaskan Arctic tundra, Global Biogeochem. Cy., 23, GB2013, doi:10.1029/2009GB003487, 2009.

BGD
10, 16491–16549, 2013

A satellite data driven biophysical modeling

J. D. Watts et al.

Zona, D., Oechel, W. C., Richards, J. H., Hastings, S., Kopetz, I., Ikawa, H., and Oberbauer, S.: Light-stress avoidance mechanisms in a Sphagnum-dominated wet coastal Arctic tundra ecosystem in Alaska, Ecology, 92, 633–644, 2011.

Zona, D., Lipson, D. A., Paw U, K. T., Oberbauer, S. F., Olivas, P., Gioli, B., and Oechel, W. C.: Increased CO_2 loss from vegetated drained lake tundra ecosystems due to flooding, Global Biogeochem. Cy., 26, GB2004, doi:10.1029/2011GB004037, 2012.

Zubrzycki, S., Kutzbach, L., Grosse, G., Desyatkin, A., and Pfeiffer, E.-M.: Organic carbon and total nitrogen stocks in soils of the Lena River Delta, Biogeosciences, 10, 3507–3524, doi:10.5194/bg-10-3507-2013, 2013.

Zürcher, S., Spahni, R., Joos, F., Steinacher, M., and Fischer, H.: Impact of an abrupt cooling event on interglacial methane emissions in northern peatlands, Biogeosciences, 10, 1963–1981, doi:10.5194/bg-10-1963-2013, 2013.

Table 1. Description of flux tower locations and site characteristics including permafrost (PF) cover and climate. The length (days) of each tower site CO_2 and CH_4 record is provided in addition to the observation year.

Site name	Location (Lat. Lon.)	Climate	Land cover	Observation period	In-situ data	Data source
Siikaneva, Finland (SK)	61°50′ N, 24°12′ E	PF: N/A MAT 3.3 °C MAP 713 mm	homogenous boreal oligotrophic fen with peat, sedges, graminoids	8 Mar–14 Nov 2005 (273 days) CO_2 (165 days) CH_4	CO_2, CH_4 5, 10 cm T_s	Aurela et al. (2007) Rinne et al. (2007) Riutta et al. (2007)
Lena River Delta, Russia (LR)	72°22′ N, 126°30′ E	PF: Continuous MAT −14.7 °C MSP 72–208 mm	wet polygonal tundra with sedges, dwarf shrubs, forbes, moss	19 Jul–21 Oct 2003 (95 days) CO_2, CH_4 9 Jun–17 Sep 2006 (101 days) CO_2, CH_4	CO_2, CH_4 5, 10 cm T_s ≤ 12 cm θ	Boike et al. (2008) Kutzbach et al. (2007) Sachs et al. (2008) Wille et al. (2008)
Zackenberg, Greenland (ZK)	74°28′ N, 20°34′ W	PF: Continuous MAT −9 °C MAP 200 mm	heterogeneous wetland fen tundra with graminoids, heath, moss	24 Jun–31 Oct 2008 (130 days) CO_2, CH_4 16 May–25 Oct 2009 (163 days) CO_2,CH_4	CO_2, CH_4 2, 5, 10 cm T_s ≤ 20 cm θ	Sigsgaard (2011) Tagesson et al. (2012)
Stordalen Mire, Sweden (SM)	68°20′ N, 19°03′ E	PF: Discontinuous MAT −0.9 °C MAP 305 mm	palsa mire with graminoids, dwarf shrubs, birch, moss, lichen	1 Jan–31 Dec 2006 (365 days) CH_4 1 Jan–31 Dec. 2007 (365 days) CH_4	CH_4 3 cm T_s	Jackowicz-Korczyński et al. (2010)
Kytalyk, Russia (KY)	70°49′ N, 147°29′ E	PF: Continuous MAT −10.5 °C MAP 220 mm	polygonal tundra with mixed shrub, sedge, moss	8 Jun–10 Aug 2009 (64 days) CO_2 5 Jul–3 Aug 2009 (30 days) CH_4	CO_2, CH_4 4, 8 cm T_s	Parmentier et al. (2011a, b)
Barrow, Alaska (BA)	71°17′ N, 156°35′ W	PF: Continuous MAT −12 °C MAP 106 mm	thaw lake basin with moss and sedge	12 Jun–31 Aug 2007 North: (81 days) CO_2 North: (46 days) CH_4	CO_2, CH_4 5, 10 cm T_s ≤ 10 cm θ	Zona et al. (2009, 2012)
				20 Aug–21 Oct 2009 North: (30, 11 days) CO_2, CH_4, Central: (12, 23 days) CO_2, CH_4 South: (2, 10 days) CO_2, CH_4	CO_2, CH_4 5 cm T_s ≤ 10 cm θ	Sturtevant et al. (2012)

BGD
10, 16491–16549, 2013

Table 2. Comparison between tower CO_2 records and TCF modeled gross primary production (GPP), ecosystem respiration (R_{eco}) and net ecosystem CO_2 exchange (NEE) derived using in-situ information (in parentheses) or MERRA and MODIS inputs. Measures of relative agreement include Pearson correlation coefficients (r) for daily and 8 day cumulative fluxes, root-mean-square-error (RMSE) and mean residual error (MRE) differences in $g\,C\,m^{-2}\,d^{-1}$. The cumulative EC record and TCF model based fluxes are also provided ($g\,C\,m^{-2}$) for each site. For MRE, negative (positive) values indicate that model results overestimate (underestimate) site EC fluxes. All r coefficients are significant at a 0.05 probability level, excluding the MODIS and MERRA based TCF model results for Kytalyk 2009 NEE ($p \geq 0.17$) and Barrow 2007-N GPP and NEE ($p \geq 0.16$).

Site	Year	Flux	r	8 day r	RMSE	MRE	Site EC total	TCF model total
Siikaneva	2005	GPP	0.84	0.94	0.8	−0.2	361.1	409.4
		R_{eco}	0.96 (0.96)	0.96 (0.98)	0.4 (0.3)	−0.3 (0.1)	289.9	365.6 (274.9)
		NEE	0.49 (0.91)	0.92 (0.92)	0.5 (0.3)	0.3 (−0.1)	−71.2	−43.8 (−86.2)
Lena River	2003	GPP	0.74	0.91	0.7	−0.1	72.3	131.5
		R_{eco}	0.77 (0.87)	0.83 (0.91)	1. (0.3)	−0.5 (−0.1)	56.3	103.3 (62.4)
		NEE	0.90 (0.94)	0.93 (0.97)	0.3 (0.3)	−0.1 (0.01)	−16.0	−28.2 (−9.9)
	2006	GPP	0.78	0.86	1.1	0.5	247.4	199.3
		R_{eco}	0.76 (0.84)	0.91 (0.91)	0.7 (0.6)	0.3 (0.2)	193.0	160 (176.4)
		NEE	0.57 (0.76)	0.62 (0.89)	0.7 (0.6)	0.2 (−0.2)	−54.4	−39.3 (−71.0)
Zackenberg	2008	GPP	0.75	0.76	1.8	< 0.1	218.2	215.4
		R_{eco}	0.67 (0.44)	0.80 (0.50)	1.1 (1.3)	0.3 (0.3)	215.9	175.5 (182.6)
		NEE	0.31 (0.83)	0.37 (0.85)	1.7 (1.3)	−0.3 (−0.3)	−2.3	−39.9 (−35.6)
	2009	GPP	0.91	0.96	1.3	0.6	305.0	234.6
		R_{eco}	0.86 (0.90)	0.93 (0.96)	0.8 (1)	0.4 (0.01)	250.3	183.7 (238.6)
		NEE	0.89 (0.89)	0.92 (0.92)	1.2 (1)	0.2 (−0.1)	−54.7	−50.9 (−66.4)
Kytalyk	2009	GPP	0.41	0.73	2.2	−1.5	143.2	224.9
		R_{eco}	0.49 (0.60)	0.80 (0.94)	1.6 (1.3)	−2.2 (−15)	60.8	200.2 (126.9)
		NEE	0.11 (0.92)	0.01 (0.95)	1.6 (1.3)	0.9 (15)	−82.4	−24.7 (−16.3)
Barrow	2007-N	GPP	0.12	0.32	1.1	0.2	152.0	137.0
		R_{eco}	0.23 (0.61)	0.64 (0.82)	0.5 (0.4)	0.4 (−0.1)	117.4	104.3 (121.6)
		NEE	0.10 (0.79)	0.20 (0.79)	0.8 (0.4)	< 0.1 (0.01)	−34.6	−32.7 (−30.4)
	2009-N	NEE	–	–	1.6	1.4	−62.1	−15.6
	2009-C	NEE	–	–	0.5	0.4	−8.3	−3.6

BGD
10, 16491–16549, 2013

Table 3. Comparison between tower CH_4 observations and TCF model simulation results using in-situ information (in parentheses) or MERRA and MODIS inputs. Measures of relative agreement include Pearson correlation coefficients (r) for daily and 8 day cumulative fluxes, root-mean-square-error (RMSE) and mean residual error (MRE) differences in $\mathrm{mg\,C\,m^{-2}\,d^{-1}}$. The cumulative EC record and TCF model based fluxes are also provided ($\mathrm{mg\,C\,m^{-2}}$) for each site. For MRE, negative (positive) values indicate that model results overestimate (underestimate) site EC fluxes. Model results for Barrow correspond to northern (N), central (C), and southern (S) tower locations. All r coefficients are significant at a 0.05 probability level, excluding the TCF model results for the Kytalyk 2009 daily fluxes ($p \geq 0.07$).

Site	Year	r	8 day r	RMSE	MRE	Site EC total	TCF model total
Siikaneva	2005	0.72 (0.75)	0.90 (0.90)	21.8 (16.9)	−9.6 (−1.2)	5.9	7.6 (6.3)
Lena River	2003	0.59 (0.87)	0.88 (0.97)	9.1 (7.5)	4.7 (0.5)	1.4	0.9 (1.2)
	2006	0.53 (0.69)	0.81 (0.78)	6.9 (9.3)	−1.3 (−4.4)	1.4	1.6 (1.9)
Zackenberg	2008	0.78 (0.84)	0.91 (0.95)	35.7 (28.5)	11.6 (2.4)	7.6	6.1 (7.3)
	2009	0.75 (0.88)	0.84 (0.95)	28.7 (21.2)	−1.1 (−6.7)	6.3	6.5 (7.4)
Stordalen Mire	2006	0.80 (0.80)	0.88 (0.89)	35 (33.4)	13.3 (0.9)	18.3	12.6 (17.9)
	2007	0.80 (0.79)	0.94 (0.89)	39.4 (42.5)	12.6 (−5.3)	22.1	17.5 (23.9)
Kytalyk	2009	0.28 (0.24)	0.66 (0.41)	20.1 (14.9)	−6.4 (0.7)	0.9	1.1 (0.8)
Barrow	2007N	0.51 (0.78)	0.94 (0.80)	5.8 (6.7)	−1.5 (−2.4)	0.7	0.8 (0.9)
	2009N	–	–	4.5 (15.9)	−0.5 (−12.6)	0.1	0.1 (0.2)
	2009C	–	–	4.2 (10.2)	0.4 (−4.7)	0.2	0.3 (0.3)
	2009S	–	–	7.2 (7.6)	−0.2 (6.3)	0.2	0.2 (0.2)

BGD
10, 16491–16549, 2013

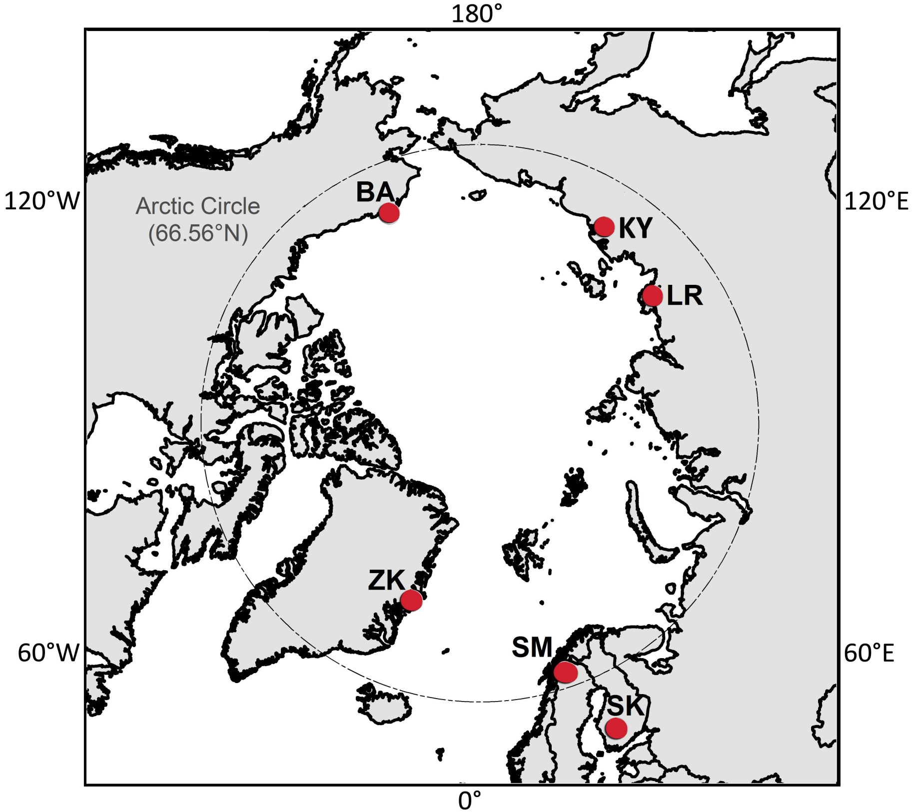

Fig. 1. Locations of flux tower sites (circles) used in this investigation, including Barrow (BA), Kytalyk (KY), Lena River (LR), Siikaneva (SK), Stordalen Mire (SM) and Zackenberg (ZK). The Arctic Circle is indicated by the dashed line.

BGD
10, 16491–16549, 2013

A satellite data driven biophysical modeling

J. D. Watts et al.

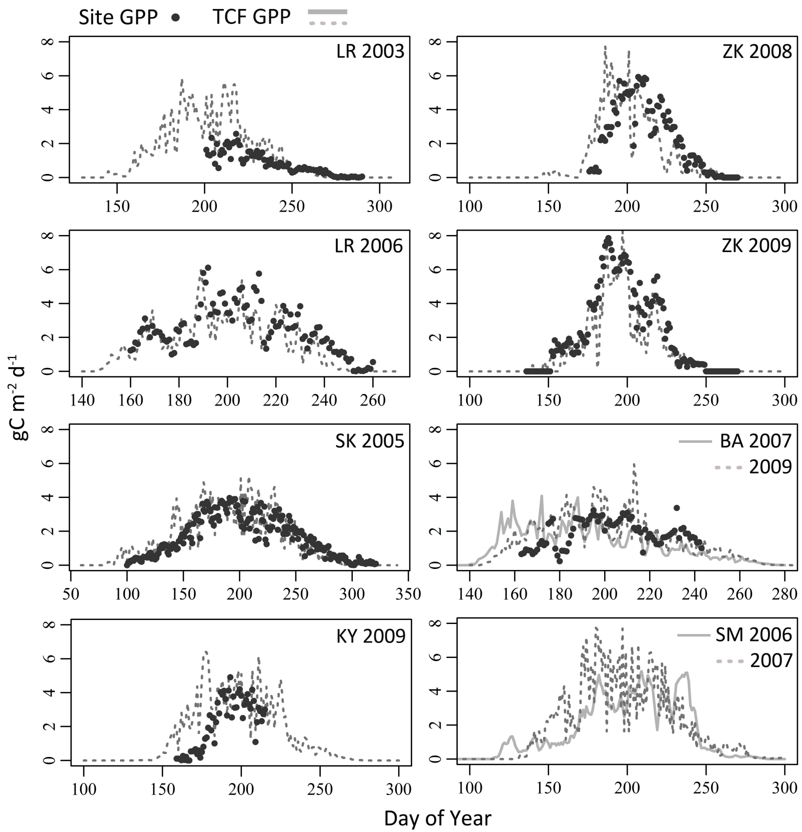

Fig. 2. TCF model simulations for GPP (lines; in gray) using input MODIS satellite optical and MERRA reanalysis information as compared with flux tower EC records (circles). Site GPP records were not available for SM and BA 2009.

BGD

10, 16491–16549, 2013

A satellite data driven biophysical modeling

J. D. Watts et al.

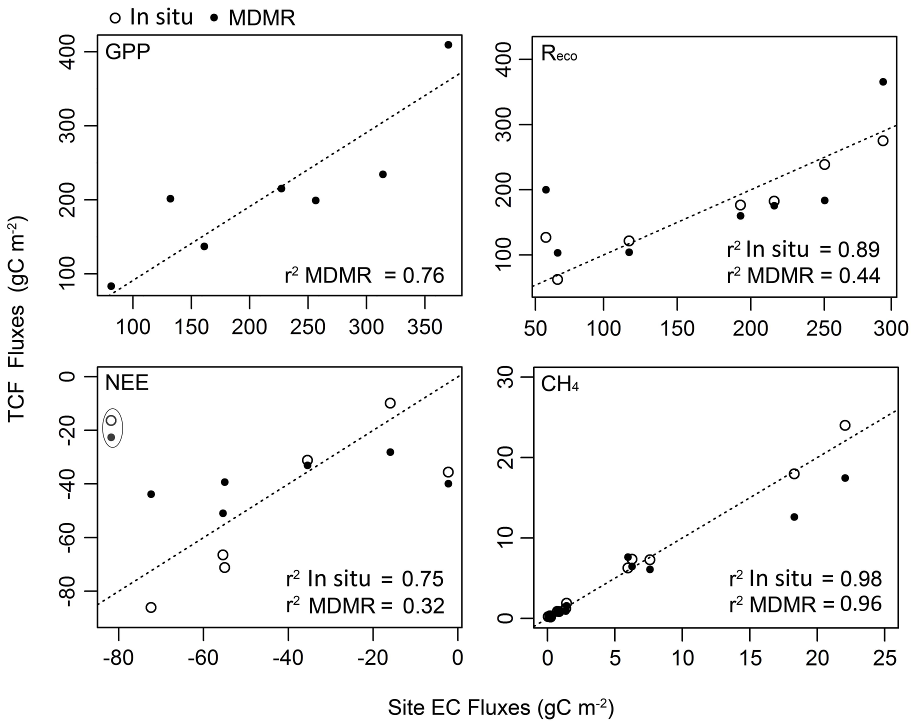

Fig. 3. Correspondence between TCF model results and EC records for cumulative ($\mathrm{g\,C\,m^{-2}}$) GPP, R_{eco}, NEE, and CH_4 fluxes from six flux tower locations. The TCF model simulations using in-situ measurements are indicated by the open circles; those using MODIS satellite optical and MERRA reanalysis information (MDMR) are shown in black. The dashed line indicates a 1 : 1 relationship between the site records and TCF model estimates. The NEE fluxes for KY (circled) were not included in the r^2 estimates due to large differences in CO_2 response relative to the other tower sites. Agreement between the TCF model simulations and tower EC records is significant at a 0.05 probability level for all comparisons, except for the MDMR based R_{eco} and NEE results where $p = 0.16$ and 0.27 respectively.

BGD
10, 16491–16549, 2013

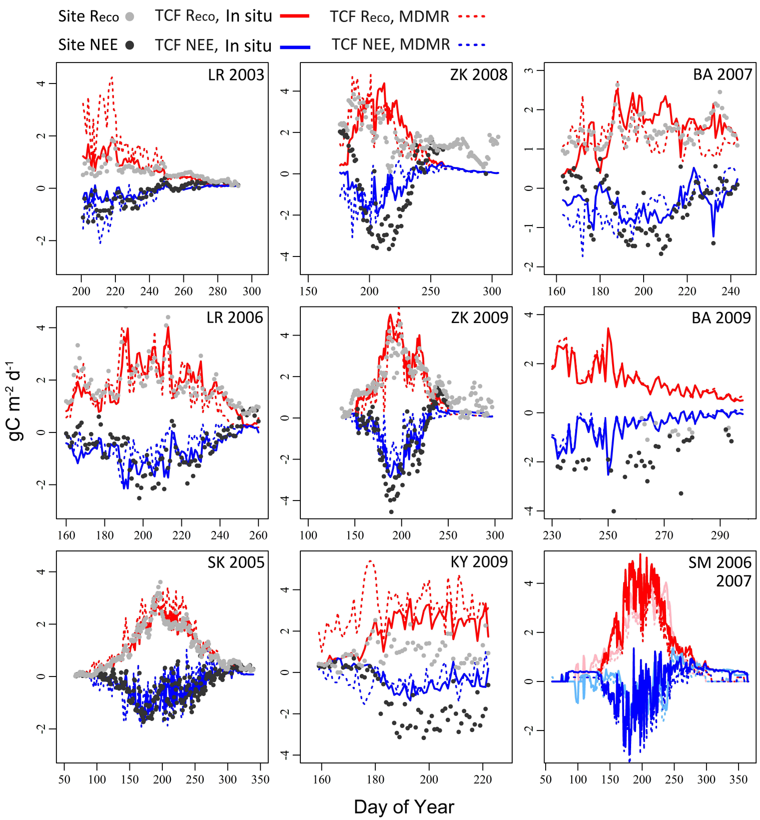

Fig. 4. TCF model CO_2 simulations using in situ (solid lines) or input MODIS satellite optical and MERRA reanalysis (MDMR; dashed lines) information, as compared with tower EC records (circles) for R_{eco} and NEE. Negative NEE values represent net daily CO_2 sink and positive NEE indicates net CO_2 source. For BA 2009, in-situ R_{eco} was not available; NEE measurements from the northern (central) tower are shown in black (grey). The TCF model R_{eco} results for SM 2006 (2007) are displayed in light (dark) red and NEE is shown in light (dark) blue.

BGD
10, 16491–16549, 2013

A satellite data driven biophysical modeling

J. D. Watts et al.

BGD
10, 16491–16549, 2013

A satellite data driven biophysical modeling

J. D. Watts et al.

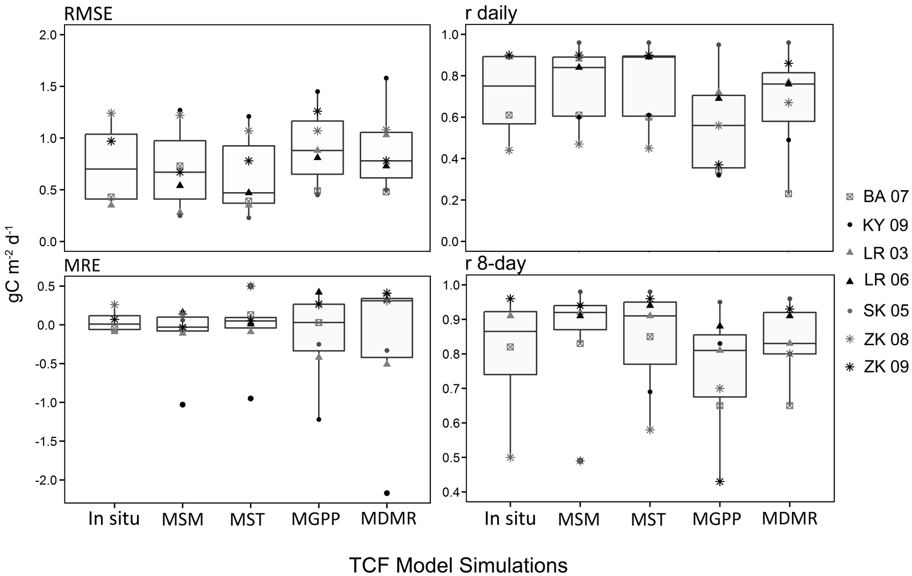

Fig. 5. TCF model accuracy for R_{eco} relative to CO_2 records from five high latitude EC tower sites. The TCF model simulations include those using information from: in-situ measurements; MERRA reanalysis soil moisture (MSM), soil temperature (MST) or TCF simulated GPP (MGPP) used in place of in-situ data; exclusively MODIS satellite optical and MERRA reanalysis drivers (MDMR). Measures of comparison include root mean squared error (RMSE), mean residual error (MRE), Pearson correlation coefficients (r) for daily and 8 day cumulative flux. Positive (negative) MRE indicates that TCF model R_{eco} is biased lower (higher) than the tower records. The BA 2009 results are means for the north, central and southern tower locations.

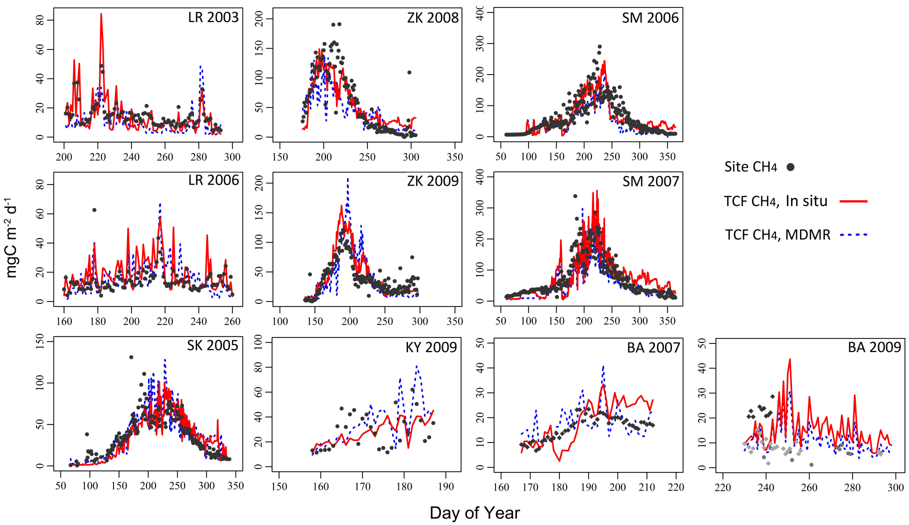

Fig. 6. TCF model CH_4 simulations using site in situ (solid lines) or input MODIS satellite optical and MERRA reanalysis (dashed lines) information, as compared with tower EC records (circles). Site observations for BA 2007 are from the northern tower location. For BA 2009, the TCF model results are simulation means for the three tower sites; diamond shapes indicate site CH_4 flux observations from the northern (in dark gray) and central (in light gray) towers whereas the gray circles indicate observations from the southern tower.

BGD
10, 16491–16549, 2013

A satellite data driven biophysical modeling

J. D. Watts et al.

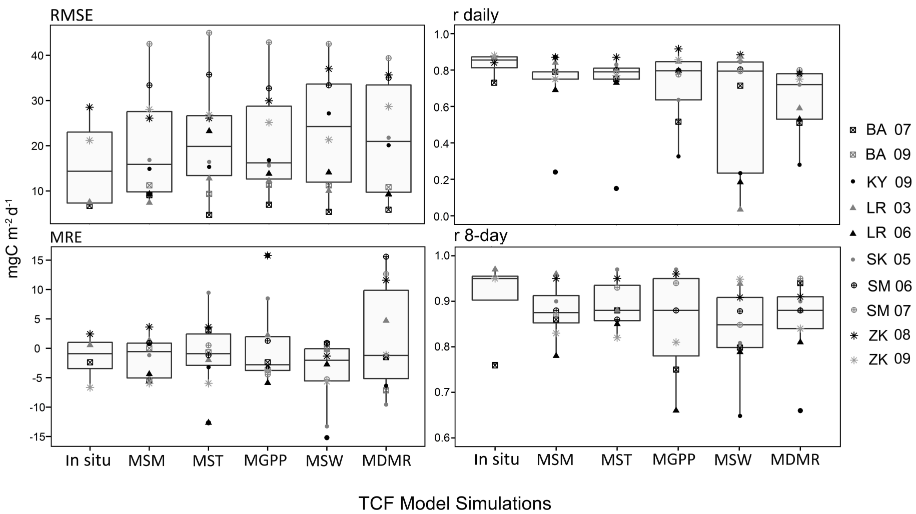

Fig. 7. TCF model accuracy relative to CH_4 records from six high latitude EC towers. Model simulations include those using information from: in-situ measurements; MERRA reanalysis soil moisture (MSM), soil temperature (MST), surface wind velocity (MSW) or model simulated GPP (MGPP) used in place of in-situ data; exclusively MODIS satellite optical and MERRA reanalysis drivers (MDMR). Measures of comparison include root mean squared error (RMSE), mean residual error (MRE), Pearson correlation coefficients (r) for daily and 8 day cumulative flux. Positive (negative) MRE indicates that TCF-based CH_4 is biased lower (higher) than tower records. Results for BA 2009 are means for north, central and southern tower locations.

BGD
10, 16491–16549, 2013

A satellite data driven biophysical modeling

J. D. Watts et al.

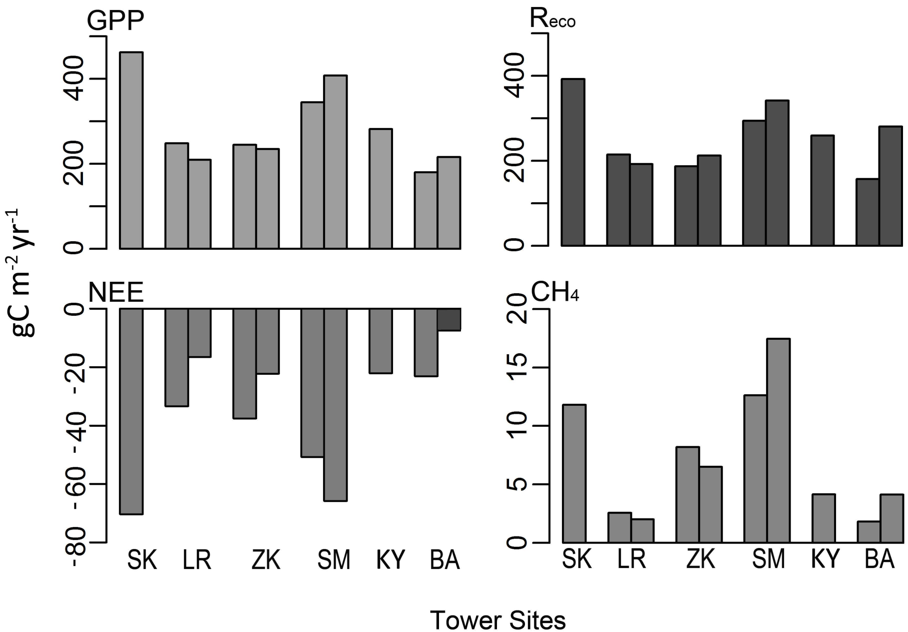

Fig. 8. The TCF model simulation results for annual cumulative GPP, R_{eco}, NEE and CH_4 emissions when using MODIS satellite optical and MERRA reanalysis inputs. For NEE, all sites are net CO_2 sinks with exception of BA 2009 which is a carbon source (in black). The years of observation for the six tower sites are: SK (2005), LR (2003, 2006), ZK (2008, 2009), SM (2006, 2007), KY (2009) and BA (2007, 2009).

BGD
10, 16491–16549, 2013